Received: 13 October 2020 | Accepted: 23 October 2020

DOI: 10.1111/sapm.12353

ORIGINAL ARTICLE

STUDIES IN APPLIED MATHEMATICS WILEY

Linear stability of transversely modulated finite-amplitude capillary waves on deep water

Sunao Murashige[1] | **Wooyoung Choi**[2]

[1] Department of Mathematics and Informatics, Ibaraki University, Mito, Ibaraki, Japan

[2] Department of Mathematical Sciences, New Jersey Institute of Technology, Newark, New Jersey

Correspondence
Sunao Murashige, Department of Mathematics and Informatics, Ibaraki University, Mito, Ibaraki, 310-8512, Japan.
Email: sunao.murashige.sci@vc.ibaraki.ac.jp

Funding information
JSPS KAKENHI, Grant/Award Number: JP17H02856; U.S. National Science Foundation, Grant/Award Number: OCE-1634939

Abstract

We investigate the three-dimensional linear stability of the periodic motion of pure capillary waves progressing in permanent form on water of infinite depth for the whole range of wave amplitudes. After introducing a coordinate transformation based on a conformal map for two-dimensional steady capillary waves, we perform linear stability analysis of finite-amplitude capillary waves in the transformed space. To solve the linearized equations for small amplitude disturbances, it is assumed that the wavelengths of the disturbances in the transverse direction are much longer than those in the propagation direction and, therefore, the disturbances are weakly three-dimensional. This assumption along with the periodicity of solutions allows us to write the linearized equations as an eigenvalue problem in matrix form. Following a perturbation theory for matrices, we expand the solutions of this eigenvalue problem in terms of a small parameter measuring the weak three-dimensionality, and numerically obtain approximate eigenvalues. For weakly three-dimensional superharmonic disturbances, the numerical results demonstrate that the pure capillary waves are two-dimensionally stable, but three-dimensionally unstable for almost all wave amplitudes. On the other hand, for subharmonic disturbances that are known to be two-dimensionally unstable, it is found that the long-wavelength disturbances in the transverse direction reduce the two-dimensional growth rate near the critical amplitude beyond which the pure capillary waves are unstable.

KEYWORDS
capillary waves, conformal mapping, numerical method, perturbation method, stability

1 | INTRODUCTION

The three-dimensional linear stability of the periodic motion of finite-amplitude water waves progressing in permanent form with constant speed has been studied previously by various authors, for example, McLean,[1] Kharif and Ramamonjiarisoa,[2] and Francius and Kharif[3] for pure gravity waves; Chen and Saffman[4] for pure capillary waves; and Zhang and Melville[5] for gravity-capillary waves (see Ref. 6 for review). They investigated the linear stability using almost the same numerical method based on Floquet theory. In this method, a small disturbance added to the periodic wave motion is approximated by a truncated series in the physical space, and the linearized equation for the disturbance is formulated as an eigenvalue problem to determine the stability. However, the convergence rate of this series depends on the wave steepness $h = H/\lambda$, where H and λ denote the crest-to-trough wave height and the wavelength, respectively. In particular, in the case of pure capillary waves, as h increases, the convergence becomes so slow that the applicable range of their numerical method is limited to small-amplitude waves with $h \leq 0.1$[4] although the maximum wave steepness of pure capillary waves is approximately 0.73.[7] In fact, the wave profiles of large-amplitude capillary waves can overhang and, then, need to be represented by a multi-valued function in the Cartesian coordinate system. Therefore, for large-amplitude capillary waves, the stability analysis in the physical space is difficult and a different approach needs to be adopted.

As an alternative, the method of conformal mapping has been successfully applied to the two-dimensional linear stability analysis of large-amplitude waves, for example, by Longuet-Higgins[8,9] and Tanaka[10] for pure gravity waves, Hogan[11] and Tiron and Choi[12] for pure capillary waves, and Murashige and Choi[13] for gravity waves on a linear shear current. In particular, Tiron and Choi[12] successfully investigated, for all wave amplitudes, the two-dimensional stability of the capillary wave solution of Crapper,[7] who analytically obtained a closed-form exact solution in a conformally mapped complex plane. Their conclusion was that Crapper's capillary waves are always stable to superharmonic disturbances, namely, small disturbances whose wavelengths are less than or equal to Crapper's wave periods, for all wave amplitudes, while they are unstable to subharmonic disturbances when the wave amplitude is greater than a critical value.

Although the application of conformal mapping is in general limited to two-dimensional problems, we try to perform the three-dimensional linear stability analysis of pure capillary waves for the whole range of the wave steepness h by introducing a coordinate transformation based on Crapper's solution. To solve the linearized equations in the transformed coordinate system, we assume that the wavelengths of small disturbances in the transverse direction (perpendicular to the wave propagation direction) are long, similarly to the transverse stability analysis for solitary waves by Kataoka and Tsutahara.[14] This assumption of long-wavelength disturbances in the transverse direction along with their periodicity in the wave propagation direction enables us to rewrite the linearized equations for three-dimensional disturbances as an eigenvalue problem in matrix form. Following a perturbation theory for matrices or linear operators [Ref. 15, section 1.6][16,17] we numerically obtain approximate solutions of this eigenvalue problem.

The paper is organized as follows. The coordinate transformation for the three-dimensional linear stability analysis is presented in Section 2. The linearized equations for small disturbances are derived in Section 3. A perturbative method to obtain approximate eigensolutions of the linearized equations is shown in Section 4. Numerical examples are presented and discussed in Section 5. Section 6 concludes this work.

2 | COORDINATE TRANSFORMATION

2.1 | Governing equations in the physical space

Assume that the fluid is inviscid and incompressible, the flow is irrotational, and the gravity effect is negligible. Consider the periodic motion of pure capillary waves progressing in permanent form with constant speed c on water of infinite depth, as shown in Figure 1(A). These two-dimensional waves are referred to as "steady capillary waves" or just "steady waves" in this paper as the wave motion is steady in the frame of reference moving with the waves, namely, in the rectangular coordinate system (x_1, x_2, y) in Figure 1(A). To study the linear stability of steady capillary waves, we add small time-dependent three-dimensional disturbances to the steady waves. Then, the irrotational fluid motion becomes unsteady and is determined by the velocity potential $\phi = \phi(x_1, x_2, y, t)$ and the wave elevation $\tilde{y}(x_1, x_2, t)$. The governing equations including the boundary conditions at the bottom $y \to -\infty$ and the water surface $y = \tilde{y}(x_1, x_2, t)$ are given by

$$\phi_{x_1x_1} + \phi_{x_2x_2} + \phi_{yy} = 0 \quad \text{for } -\infty < y < \tilde{y}(x_1, x_2, t), \tag{1}$$

$$\phi \;\to\; c\,x \quad \text{as } y \to -\infty, \tag{2}$$

$$\tilde{y}_t + \phi_{x_1}\tilde{y}_{x_1} + \phi_{x_2}\tilde{y}_{x_2} = \phi_y \quad \text{at } y = \tilde{y}(x_1, x_2, t), \tag{3}$$

$$\phi_t + \frac{1}{2}\left({\phi_{x_1}}^2 + {\phi_{x_2}}^2 + {\phi_y}^2\right) - \frac{T}{\varrho}\kappa = B(t) \quad \text{at } y = \tilde{y}(x_1, x_2, t), \tag{4}$$

where T is the surface tension, ϱ is the fluid density,

$$\kappa = \frac{(1+\tilde{y}_{x_1}^2)\tilde{y}_{x_2x_2} + (1+\tilde{y}_{x_2}^2)\tilde{y}_{x_1x_1} - 2\tilde{y}_{x_1}\tilde{y}_{x_2}\tilde{y}_{x_1x_2}}{(1+\tilde{y}_{x_1}^2+\tilde{y}_{x_2}^2)^{3/2}}, \tag{5}$$

and an arbitrary function $B(t)$ can be absorbed into ϕ. The free surface boundary conditions (3) and (4) correspond to the kinematic and dynamic conditions, respectively. Furthermore, similarly to the previous studies in Refs. 4, 12, we normalize each variable using the characteristic wavelength λ_0 and time t_0 defined by

$$\lambda_0 \;:=\; \frac{\lambda}{2\pi} \quad \text{and} \quad t_0 \;:=\; \sqrt{\left(\frac{\lambda}{2\pi}\right)^3 \frac{\varrho}{T}}\;, \tag{6}$$

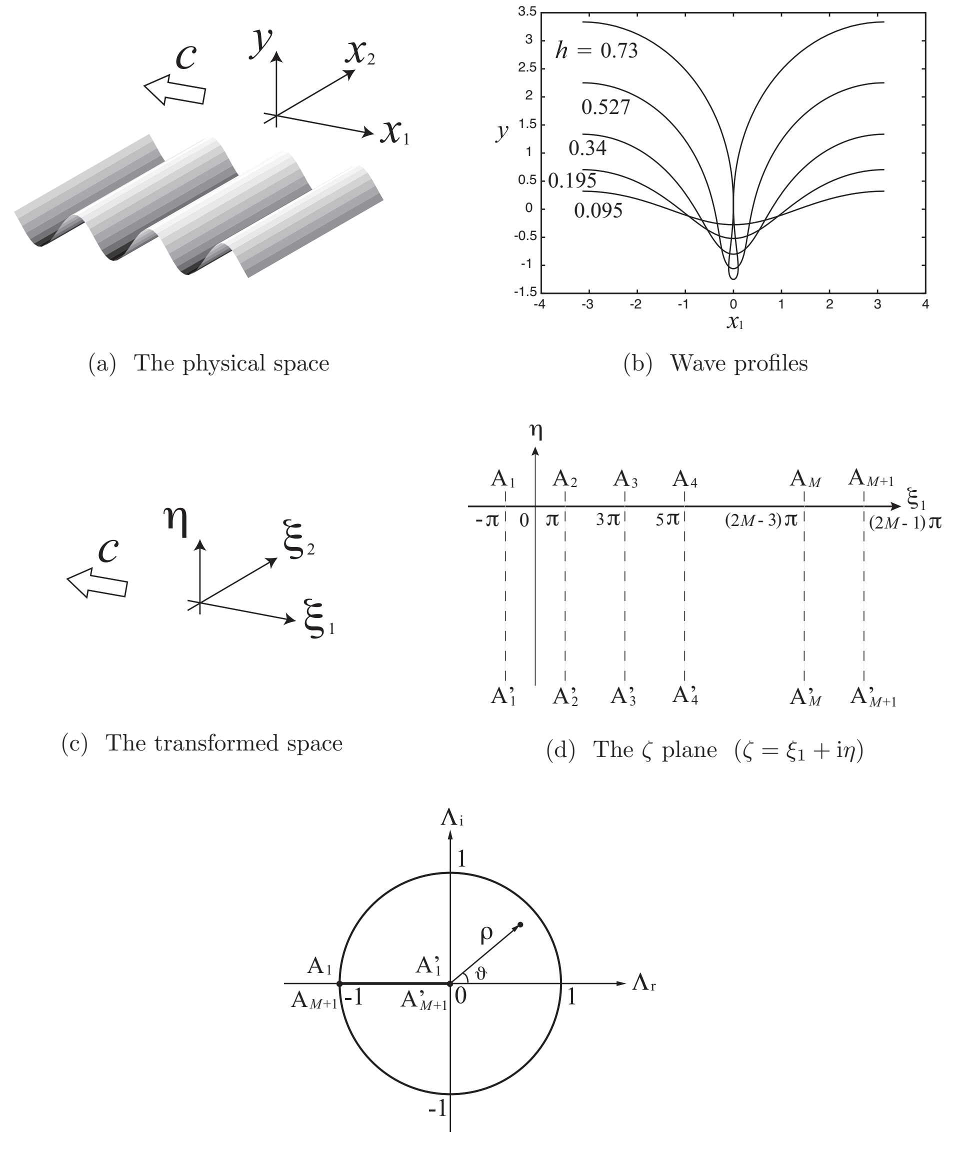

(a) The physical space

(b) Wave profiles

(c) The transformed space

(d) The ζ plane $(\zeta = \xi_1 + \mathrm{i}\eta)$

(e) The Λ plane $(\Lambda = \Lambda_r + \mathrm{i}\Lambda_i = \rho\,\mathrm{e}^{\mathrm{i}\vartheta})$

FIGURE 1 Coordinate transformations for pure capillary waves progressing on water of infinite depth. Transformation from (x_1, x_2, y) in (A) to (ξ_1, ξ_2, η) in (C) is given by (11). Conformal mapping from the ζ-plane for $p = K/M$ in (D) to the Λ-plane in (E) is given by (28) and p is defined by (27). Wave profiles in (B) for one period are computed by using Crapper's solution (8) for different values of the wave steepness $h = H/\lambda$, where H and λ denote the crest-to-trough wave height and the wavelength, respectively

as

$$x_j = \lambda_0 x_{j*} \ (j = 1, 2), \ \ y = \lambda_0 y_*, \ \ t = t_0 t_*, \ \ c = \frac{\lambda_0}{t_0} c_*, \ \ \phi = \frac{\lambda_0{}^2}{t_0} \phi_*, \tag{7}$$

where λ is the wavelength of the steady wave. Henceforth, the asterisks for dimensionless variables will be omitted for brevity.

2.2 | Coordinate transformation using Crapper's solution

Crapper[7] found that the exact solution of the irrotational plane motion of steady capillary waves on water of infinite depth is given by

$$z = Z(\zeta) = X(\xi_1, \eta) + \mathrm{i}Y(\xi_1, \eta) = \zeta + \mathrm{i}\frac{4A\mathrm{e}^{-\mathrm{i}\zeta}}{1 - A\mathrm{e}^{-\mathrm{i}\zeta}}, \tag{8}$$

with

$$\zeta = \xi_1 + \mathrm{i}\eta = \frac{1}{c} f, \tag{9}$$

and

$$A = \frac{2}{\pi h}\left\{\sqrt{1 + \left(\frac{\pi h}{2}\right)^2} - 1\right\} \quad \text{and} \quad c = \left\{1 + \left(\frac{\pi h}{2}\right)^2\right\}^{-1/4}, \tag{10}$$

where $z = x_1 + \mathrm{i}y$ is the complex coordinate, $f = \phi + \mathrm{i}\psi$ is the complex velocity potential, and $h = H/\lambda$ denotes the wave steepness (H: the crest-to-trough wave height). In the ζ-plane ($\zeta = \xi_1 + \mathrm{i}\eta$), the flow domain is conformally mapped onto the lower half $\eta < 0$ and the water surface is located on $\eta = 0$. Figure 1(B) shows the wave profiles $y = \tilde{y}_0(x_1)$ of the steady capillary waves over one wave period given by (8) for different values of h. Near the maximum wave steepness $h_{\max} \approx 0.73$, overhanging wave profiles are observed and the corresponding wave elevation $y = \tilde{y}_0(x_1)$ becomes multivalued.

It should be remarked that Crapper's capillary wave solution (8) can be considered as a conformal mapping from the ζ ($= \xi_1 + \mathrm{i}\eta$) plane to the z ($= x + \mathrm{i}y$) plane. We then use this mapping to introduce a three-dimensional coordinate transformation from (x_1, x_2, y) to (ξ_1, ξ_2, η) as

$$x_1 = X(\xi_1, \eta), \quad x_2 = \xi_2, \quad y = Y(\xi_1, \eta), \quad \text{and} \quad t = t, \tag{11}$$

where $X(\xi_1, \eta) + \mathrm{i}Y(\xi_1, \eta)$ is Crapper's solution (8). One advantage of this transformation is that, in the (ξ_1, ξ_2, η) space, the water surface $y = \tilde{y}_0(x_1)$ of steady Crapper's waves is mapped onto the plane $\eta = 0$, as shown in Figure 1(C), while the perturbed water surface $y = \tilde{y}_0(x_1) + \tilde{y}'(x_1, x_2, t)$ due to small disturbances $\tilde{y}'$ is represented in the transformed space by

$$\eta = \tilde{\eta}(\xi_1, \xi_2, t). \tag{12}$$

Also, the perturbed velocity potential $\phi = \phi(x_1(\xi_1, \eta), x_2 = \xi_2, y(\xi_1, \eta), t) = \hat{\phi}(\xi_1, \xi_2, \eta, t)$ can be represented by

$$\hat{\phi}(\xi_1, \xi_2, \eta, t) = c\,\xi_1 + \hat{\phi}'(\xi_1, \xi_2, \eta, t), \tag{13}$$

where the first term $c\,\xi_1$ on the right-hand side corresponds to the steady wave solution. For small disturbances, the perturbed solutions $\tilde{\eta}(\xi_1, \xi_2, t)$ in (12) and $\hat{\phi}'(\xi_1, \xi_2, \eta, t)$ in (13) can be assumed to be small.

3 | LINEARIZED EQUATIONS FOR SMALL DISTURBANCES

For the three-dimensional linear stability analysis of Crapper's capillary waves, we assume that the perturbed solutions $\tilde{\eta}(\xi_1, \xi_2, t)$ in (12) and $\hat{\phi}'(\xi_1, \xi_2, \eta, t)$ in (13) due to small disturbances can be separated as

$$\tilde{\eta}'(\xi_1, \xi_2, t) = \mathrm{e}^{\sigma t}\, \mathrm{e}^{\mathrm{i}q\xi_2}\, \check{\eta}(\xi_1) \quad \text{and} \quad \hat{\phi}'(\xi_1, \xi_2, \eta, t) = \mathrm{e}^{\sigma t}\, \mathrm{e}^{\mathrm{i}q\xi_2}\, \check{\phi}(\xi_1, \eta), \tag{14}$$

where $\sigma = \sigma_\mathrm{r} + \mathrm{i}\sigma_\mathrm{i} \in \mathbb{C}$, and $q > 0$ denotes the wavenumber of the disturbances in the direction transverse to the propagation direction of the steady waves. Here, the real part σ_r of σ represents the growth rate of the disturbances and the instability corresponds to $\sigma_\mathrm{r} > 0$. In this section, we derive the linearized equations for the small perturbations $\check{\eta}(\xi_1)$ and $\check{\phi}(\xi_1, \eta)$ in (14).

3.1 | Linearized equations in the ζ-plane

The governing equations (1), (2), (3), and (4) can be transformed into the (ξ_1, ξ_2, η)-space using (11). We can substitute (12) and (13) with (14) into the transformed equations, and linearize them around the steady wave solutions with respect to the small perturbations $\check{\eta}(\xi_1)$ and $\check{\phi}(\xi_1, \eta)$ in (14). The linearized equations for $\check{\eta}(\xi_1)$ and $\check{\phi}(\xi_1, \eta)$ can be written as

$$\check{\phi}_{\xi_1\xi_1} + \check{\phi}_{\eta\eta} - q^2 J \check{\phi} = 0 \quad \text{for } -\infty < \eta < 0, \tag{15}$$

$$\check{\phi} \;\to\; 0 \quad \text{as } \eta \to -\infty, \tag{16}$$

$$\sigma\check{\eta} + \frac{c}{J}\check{\eta}_{\xi_1} - \frac{1}{J}\check{\phi}_\eta = 0 \quad \text{at } \eta = 0, \tag{17}$$

$$\sigma\check{\phi} + \frac{c}{J}\check{\phi}_{\xi_1} - \mathcal{K}[\check{\eta}] + q^2\sqrt{J}\,\check{\eta} = 0 \quad \text{at } \eta = 0, \tag{18}$$

where $J = J(\xi_1, \eta)$ is defined using Crapper's solution (8) by

$$J = \frac{\partial(X, Y)}{\partial(\xi_1, \eta)} = {X_{\xi_1}}^2 + {Y_{\xi_1}}^2, \tag{19}$$

and

$$\mathcal{K}[\check{\eta}] = \alpha_0(\xi_1)\check{\eta} + \alpha_1(\xi_1)\check{\eta}_{\xi_1} + \alpha_2(\xi_1)\check{\eta}_{\xi_1\xi_1}, \tag{20}$$

with

$$\alpha_0(\xi_1) = \frac{1}{2\sqrt{J}}\left\{ \frac{c^4}{2}\left(\frac{J^2 - 1}{J}\right) + \frac{\partial}{\partial\xi_1}\left(\frac{J_{\xi_1}}{J}\right)\right\}, \quad \alpha_1(\xi_1) = \frac{J_{\xi_1}}{2J^{3/2}}, \quad \alpha_2(\xi_1) = \frac{1}{\sqrt{J}}. \tag{21}$$

In the absence of transverse perturbations, namely, for $q = 0$, these linearized equations (15), (16), (17), and (18) determine the two-dimensional linear stability of Crapper's solutions, similarly to Refs. 11, 12. In this case, from Floquet theory, the perturbations $\check{\eta}(\xi_1)$ and $\check{\phi}(\xi_1, \eta)$ can be expressed as

$$\check{\eta}(\xi_1) = \sum_{n=-\infty}^{\infty} \tilde{a}_n e^{i(p+n)\xi_1} \quad \text{and} \quad \check{\phi}(\xi_1, \eta) = \sum_{\substack{n=-\infty \\ p+n\neq 0}}^{\infty} \tilde{b}_n e^{i(p+n)\xi_1} e^{|p+n|\eta}, \tag{22}$$

where p is an arbitrary real number. Because there is a degeneracy in the choice of p [Ref. 4, p. 128], the range of p can be restricted to $0 \le p < 1$ where $p = 0$ and $0 < p < 1$ correspond to superharmonic and subharmonic cases, respectively.

On the other hand, in the zero-amplitude limit $h \to 0$, both J in (19) and the wave speed c approach unity, namely,

$$J \to 1 \quad \text{and} \quad c \to 1 \qquad \text{as } h \to 0. \tag{23}$$

In this limit, the general solutions of the linearized equations (15), (16), (17), and (18) can be written in the form

$$\check{\eta}(\xi_1) = \sum_{n=-\infty}^{\infty} \tilde{a}_n e^{i(p+n)\xi_1} \quad \text{and} \quad \check{\phi}(\xi_1, \eta) = \sum_{\substack{n=-\infty \\ p+n\neq 0}}^{\infty} \tilde{b}_n e^{i(p+n)\xi_1} e^{\sqrt{(p+n)^2+q^2}\cdot\eta}, \tag{24}$$

and the eigenvalue σ is given by

$$\sigma = \sigma_n^{\pm}(p, q) \ := \ -i\Big[p + n \pm \big\{(p+n)^2 + q^2\big\}^{3/4}\Big], \tag{25}$$

where p and q are arbitrary real numbers. This result agrees with that by Chen and Saffman [Ref. 4, eq. (2.15a) on p. 129].

In the general case of finite-amplitude steady waves with three-dimensional disturbances ($q \neq 0$), we cannot apply the classical method developed for the previous stability analysis in the physical space as $J = J(\xi_1, \eta)$ in (15) depends on ξ_1 and η. Notice that, if we perform the stability analysis in the physical space, instead of the ζ-plane, as in [Ref. 4, section 2], the linearized equation corresponding to (15) is given by the Helmholtz equation with a constant coefficient, and the perturbed solutions can be written in the same form as (24) using Floquet theory. However, due to the slow convergence of the series expansion in the physical space, the stability analysis is limited to small-amplitude waves, as discussed in Section 1.

In this work, similarly to Ref. 9, we assume that $\check{\eta}(\xi_1)$ and $\check{\phi}(\xi_1, \eta)$ are both $2M\pi$-periodic ($M = 1, 2, \dots$) in the propagation direction of waves, namely, with respect to ξ_1, as

$$\check{\eta}(\xi_1) = \check{\eta}(\xi_1 + 2M\pi) \quad \text{and} \quad \check{\phi}(\xi_1, \eta) = \check{\phi}(\xi_1 + 2M\pi, \eta) \quad \text{with } M = 1, 2, \dots . \tag{26}$$

This assumption corresponds to the case of the wavenumber p in (22) or (24) being a rational number given by

$$p = K/M \qquad \text{with} \quad K = 0, 1, \dots, M-1. \tag{27}$$

In addition, we assume that the transverse wavenumber q is small, namely, the wavelength of small disturbances being long, and use q as a perturbation parameter. However, the perturbative expansion of the dependent variables σ, $\check{\eta}$, and $\check{\phi}$ depends on the multiplicity of the leading-order eigenvalue, as will be shown in Section 4. For a systematic development of a perturbation method, we introduce another complex plane, the Λ-plane shown in Figure 1(E), and rewrite the linearized equations in matrix form in Section 3.2. In particular, the Λ-plane helps us represent $\check{\phi}$ in the integral form using the boundary value of $\check{\phi}$ on the water surface, which will be shown in Section 3.2.2.

3.2 | Linearized equations in the Λ plane

3.2.1 | Transformation of the flow domain into the Λ plane

To examine the linear stability due to small disturbances that are $2M\pi$-periodic in the propagation direction of the steady waves as in (26), we consider the flow domain in the semi-infinite strip $\mathcal{D}_M$: $-\pi < \xi_1 < (2M-1)\pi$ and $-\infty < \eta < 0$ in the ζ-plane ($\zeta = \xi_1 + \mathrm{i}\eta$) as shown in Figure 1(D), where the width $\mathrm{A}_1\mathrm{A}_{M+1}$ of the domain $\mathcal{D}_M$ is equal to $2M\pi$. This domain $\mathcal{D}_M$ can be conformally mapped onto the unit disk $|\Lambda| < 1$ in the Λ-plane ($\Lambda = \rho e^{\mathrm{i}\vartheta}$), as shown in Figure 1(E), using

$$\log\Lambda = -\mathrm{i}\left(\frac{\zeta+\pi}{M} - \pi\right), \tag{28}$$

or

$$\rho = e^{\eta/M} \quad \text{and} \quad \vartheta = -\left(\frac{\xi_1+\pi}{M} - \pi\right) \qquad \text{with} \quad \Lambda = \rho e^{\mathrm{i}\vartheta} \quad \textit{and} \quad \zeta = \xi_1 + \mathrm{i}\eta, \tag{29}$$

where a branch cut is set to $-\infty < \Lambda \le 0$ along the real axis in the Λ-plane such that $\log\Lambda$ is uniquely defined. From the periodicity in (26), the perturbed solutions are continuous and 2π-periodic with respect to ϑ in the Λ-plane. Notice that $\rho = 1$ corresponds to the profile of Crapper's capillary wave.

Then, the linearized equations (15), (16), (17), and (18) for the perturbed solutions can be rewritten in the Λ-plane in the form

$$\nabla^2\check{\phi} \;:=\; \frac{1}{\rho}\frac{\partial}{\partial\rho}\left(\rho\frac{\partial\check{\phi}}{\partial\rho}\right) + \frac{1}{\rho^2}\check{\phi}_{\vartheta\vartheta} = q^2M^2\frac{1}{\rho^2}J\check{\phi} \qquad \text{for } |\Lambda| = \rho < 1, \tag{30}$$

$$\check{\phi} \to 0 \quad \text{as } \rho \to 0, \tag{31}$$

$$\sigma\check{\eta} - \frac{c}{J}\frac{1}{M}\check{\eta}_\vartheta - \frac{1}{J}\frac{1}{M}\check{\phi}_\rho = 0 \quad \text{at } \rho = 1, \tag{32}$$

$$\sigma\check{\phi} - \frac{c}{J}\frac{1}{M}\check{\phi}_\vartheta - \hat{\mathcal{K}}[\check{\eta}] = -q^2\sqrt{J}\,\check{\eta} \quad \text{at } \rho = 1, \tag{33}$$

with

$$\hat{\mathcal{K}}[\check{\eta}] = \alpha_0(\vartheta)\check{\eta} - \alpha_1(\vartheta)\frac{1}{M}\check{\eta}_\vartheta + \alpha_2(\vartheta)\frac{1}{M^2}\check{\eta}_{\vartheta\vartheta} \tag{34}$$

where $J(\rho,\vartheta) = J(\xi_1(\vartheta),\eta(\rho))$ and $\alpha_j(\vartheta) = \alpha_j(\xi_1(\vartheta))$ ($j = 0,1,2$) are defined by (19) and (21), respectively. For convenience, we write $\check{\eta} = \check{\eta}(\vartheta)$ and $\check{\phi} = \check{\phi}(\rho,\vartheta)$ in the Λ-plane, instead of $\check{\eta} = \check{\eta}(\xi_1(\vartheta))$ and $\check{\phi} = \check{\phi}(\xi_1(\vartheta),\eta(\rho))$.

In the absence of transverse perturbations, or for $q = 0$, (30) becomes the Laplace equation, and thus the 2π-periodic perturbations $\check{\eta}(\vartheta)$ and $\check{\phi}(\rho,\vartheta)$ with respect to ϑ can be written in the form

$$\check{\eta}(\vartheta) = \sum_{j=-\infty}^{\infty} a_j e^{ij\vartheta} \quad \text{and} \quad \check{\phi}(\rho,\vartheta) = \sum_{\substack{j=-\infty \\ j\neq 0}}^{\infty} b_j e^{ij\vartheta}\rho^{|j|}, \tag{35}$$

where $b_0 = 0$ from the bottom condition (31). Using (29), we can relate j in (35) to n in (22) by $j = j_p(n) = -M(p+n)$ and, from (27),

$$j_p(n) = -(Mn+K) \quad \text{for } \; p = K/M, \tag{36}$$

where $K = 0,1,\dots,M-1$. Then, if a natural number is chosen for M, each normal mode labelled by $j \in \mathbb{Z}$ in (35) can be classified into mutually disjoint M sets, similarly to [Ref. 9, §4], namely

$$\mathbb{Z} = U_0 \cup U_1 \cup \dots U_{M-1} \quad \text{with } \; U_{K_1} \cap U_{K_2} = \emptyset \;\; (K_1 \neq K_2), \tag{37}$$

where $\mathbb{Z}$ is a set of integers and

$$U_K \;:=\; \left\{ j_{p=K/M}(n) \right\}_{n=-\infty}^{\infty} = \{-(Mn+K)\}_{n=-\infty}^{\infty} \qquad (K = 0,1,\dots,M-1). \tag{38}$$

Note that $0 \in U_0$. For example, in the case of $M = 2$, $\mathbb{Z}$ is divided into two sets, $U_0 = \{j_{p=0}(n)\}_{n=-\infty}^{\infty} = \{-2n\}_{n=-\infty}^{\infty}$ (even numbers) and $U_1 = \{j_{p=1/2}(n)\}_{n=-\infty}^{\infty} = \{-(2n+1)\}_{n=-\infty}^{\infty}$ (odd numbers). This separation in (37) will be used to determine the stability for a specified value of $p = K/M$ in Section 3.2.2. The results are expected to be equivalent to those of Tiron and Choi,[12] which will be used to validate the current approach.

3.2.2 | Linearized equations for small values of q

For nonzero q, the solution to (30)–(33) cannot be expressed in the form of (35). To take advantage of the periodicity of perturbed solutions, it is convenient to introduce the surface potential $\check{\varphi}$ defined by

$$\check{\varphi}(\vartheta) \;:=\; \check{\phi}(\rho = 1, \vartheta). \tag{39}$$

Then, one can rewrite the linearized free surface boundary conditions (32) and (33) as the linear equations for $\check{\eta}$ and $\check{\varphi}$ after expressing $\check{\phi}_\rho = \partial\check{\phi}/\partial\rho$ in terms of $\check{\varphi}$, as discussed in the followings.

First, Green's formula for $\check{\phi}$ on the unit disk $|\Lambda| < 1$ satisfying (30) and (31) yields

$$\check{\phi}(\rho,\vartheta) = \frac{1}{2\pi}\int_{-\pi}^{\pi} [P(\rho,\vartheta-\vartheta')]\check{\varphi}(\vartheta')d\vartheta' - \int_0^1\int_{-\pi}^{\pi} [G(\Lambda;\Lambda')]\, \nabla^2\check{\phi}\cdot\rho' d\vartheta' d\rho', \tag{40}$$

where $G(\Lambda = \rho e^{i\vartheta}; \Lambda' = \rho' e^{i\vartheta'})$ is Green's function [Ref. 18, p. 659, eq. (114)] given by

$$G(\Lambda;\Lambda') = -\frac{1}{2\pi}\log\left|\frac{\Lambda-\Lambda'}{\overline{\Lambda'}\Lambda-1}\right| = -\frac{1}{4\pi}\log\left\{\frac{\rho^2-2\rho\rho'\cos(\vartheta-\vartheta')+\rho'^2}{\rho^2\rho'^2-2\rho\rho'\cos(\vartheta-\vartheta')+1}\right\}, \tag{41}$$

$P(\rho, \vartheta - \vartheta')$ is the Poisson kernel [Ref. 19, p. 91, eq. (3.49)] for the unit disc defined by

$$P(\rho,\vartheta-\vartheta') := -2\pi\left.\frac{\partial G}{\partial \rho'}\right|_{\rho'=1} = \frac{1-\rho^2}{\rho^2-2\rho\cos(\vartheta-\vartheta')+1}, \tag{42}$$

$[G(\Lambda;\Lambda')] = G(\Lambda;\Lambda') - G(\Lambda = 0;\Lambda')$, $[P(\rho,\vartheta)] = P(\rho,\vartheta) - P(\rho = 0,\vartheta)$, and $\overline{\Lambda}$ in (41) denotes the complex conjugate of Λ. Using (30), we can rewrite (40) as

$$\check{\phi}(\rho,\vartheta) = \mathcal{T}_0[\check{\varphi}](\rho,\vartheta) + q^2M^2\mathcal{S}[\check{\phi}](\rho,\vartheta), \tag{43}$$

where

$$\mathcal{T}_0[\check{\varphi}](\rho,\vartheta) := \frac{1}{2\pi}\int_{-\pi}^{\pi}[P(\rho,\vartheta-\vartheta')]\,\check{\varphi}(\vartheta')\mathrm{d}\vartheta', \tag{44}$$

and

$$\mathcal{S}[\check{\phi}](\rho,\vartheta) := -\int_0^1\int_{-\pi}^{\pi}[G(\Lambda;\Lambda')]\,J(\rho',\vartheta')\,\frac{1}{\rho'}\check{\phi}(\rho',\vartheta')\mathrm{d}\vartheta'\mathrm{d}\rho'. \tag{45}$$

For small q, using (43) recursively, we have

$$\check{\phi}(\rho,\vartheta) = \mathcal{T}_0[\check{\varphi}](\rho,\vartheta) + q^2M^2\mathcal{T}_1[\check{\varphi}](\rho,\vartheta) + q^4M^4\mathcal{T}_2[\check{\varphi}](\rho,\vartheta) + \mathrm{O}(q^6), \tag{46}$$

where

$$\mathcal{T}_1[\check{\varphi}](\rho,\vartheta) = \mathcal{S}\circ\mathcal{T}_0[\check{\varphi}](\rho,\vartheta) \quad \text{and} \quad \mathcal{T}_2[\check{\varphi}](\rho,\vartheta) = \mathcal{S}^2\circ\mathcal{T}_0[\check{\varphi}](\rho,\vartheta). \tag{47}$$

From these, Equations (32) and (33) can be rewritten as

$$\sigma\check{\eta} - \frac{c}{J}\frac{1}{M}\check{\eta}_\vartheta - \frac{1}{J}\frac{1}{M}\frac{\partial\mathcal{T}_0[\check{\varphi}]}{\partial\rho} = q^2\frac{M}{J}\frac{\partial\mathcal{T}_1[\check{\varphi}]}{\partial\rho} + q^4\frac{M^3}{J}\frac{\partial\mathcal{T}_2[\check{\varphi}]}{\partial\rho} + \mathrm{O}(q^6) \quad \text{at } \rho = 1, \tag{48}$$

$$\sigma\check{\varphi} - \frac{c}{J}\frac{1}{M}\check{\varphi}_\vartheta - \hat{\mathcal{K}}[\check{\eta}] = -q^2\sqrt{J}\,\check{\eta} \quad \text{at } \rho = 1. \tag{49}$$

This linear system for $\check{\eta}$ and $\check{\varphi}$ in (48) and (49) determines the approximate eigenvalue σ for small values of q, namely, the linear stability due to long-wavelength disturbances in the transverse direction.

Furthermore, using the periodicity and the following Galerkin's method,[5] we can arrange and simplify the linear system of (48) and (49) in the matrix form, which is suitable for the numerical evaluation of the linear system, as follows. First the 2π-periodic functions $\check{\eta}(\vartheta)$ and $\check{\varphi}(\vartheta)$ in (48) and (49) can be expanded in the form of Fourier series

$$\check{\eta}(\vartheta) = \sum_{j=-\infty}^{\infty} \check{a}_j \mathrm{e}^{\mathrm{i}j\vartheta} \quad \text{and} \quad \check{\varphi}(\vartheta) = \sum_{j=-\infty}^{\infty} \check{b}_j \mathrm{e}^{\mathrm{i}j\vartheta}. \tag{50}$$

Then, using the relation

$$\frac{1}{2\pi}\int_{-\pi}^{\pi} P(\rho, \vartheta - \vartheta')\mathrm{e}^{\mathrm{i}j\vartheta'}\mathrm{d}\vartheta' = \rho^{|j|}\mathrm{e}^{\mathrm{i}j\vartheta}, \tag{51}$$

we can rewrite $\mathcal{T}_0[\check{\varphi}]$ in (44) as

$$\mathcal{T}_0[\check{\varphi}](\rho, \vartheta) = \sum_{\substack{j=-\infty \\ j\neq 0}}^{\infty} \check{b}_j \rho^{|j|}\mathrm{e}^{\mathrm{i}j\vartheta}, \tag{52}$$

and also $\partial\mathcal{T}_i[\check{\varphi}]/\partial\rho$ $(i = 0, 1, 2)$ on $\rho = 1$ in (48), respectively, as

$$\frac{\partial\mathcal{T}_0[\check{\varphi}]}{\partial\rho} = \sum_{\substack{j=-\infty \\ j\neq 0}}^{\infty} \check{b}_j |j| \mathrm{e}^{\mathrm{i}j\vartheta}, \quad \frac{\partial\mathcal{T}_1[\check{\varphi}]}{\partial\rho} = \sum_{\substack{j=-\infty \\ j\neq 0}}^{\infty} \check{b}_j F_{1\mathrm{j}}(\vartheta), \quad \frac{\partial\mathcal{T}_2[\check{\varphi}]}{\partial\rho} = \sum_{\substack{j=-\infty \\ j\neq 0}}^{\infty} \check{b}_j F_{2\mathrm{j}}(\vartheta), \tag{53}$$

where $F_{1\mathrm{j}}(\vartheta)$ and $F_{2\mathrm{j}}(\vartheta)$ are given, respectively, by

$$F_{1\mathrm{j}}(\vartheta) = \int_0^1 \rho'^{|j|-1}\left\{\frac{1}{2\pi}\int_{-\pi}^{\pi} P(\rho', \vartheta - \vartheta')\, J(\rho', \vartheta')\, \mathrm{e}^{\mathrm{i}j\vartheta'}\mathrm{d}\vartheta'\right\}\mathrm{d}\rho' \ , \tag{54}$$

$$F_{2\mathrm{j}}(\vartheta) = \int_0^1 \frac{1}{\rho'}\left\{\frac{1}{2\pi}\int_{-\pi}^{\pi} P(\rho', \vartheta - \vartheta')\, J(\rho', \vartheta')\, \mathcal{S}[\rho'^{|j|}\mathrm{e}^{\mathrm{i}j\vartheta'}]\mathrm{d}\vartheta'\right\}\mathrm{d}\rho'. \tag{55}$$

Substituting these into (48) and (49), we obtain

$$\sum_{j=-\infty}^{\infty} \check{a}_j\left\{\sigma\mathrm{e}^{\mathrm{i}j\vartheta} - \check{L}_j^{(1a)}(\vartheta)\right\} - \sum_{\substack{j=-\infty \\ j\neq 0}}^{\infty} \check{b}_j \check{L}_j^{(1b)}(\vartheta) = \sum_{\substack{j=-\infty \\ j\neq 0}}^{\infty} \check{b}_j\left\{q^2\check{B}_{1j}^{(1b)}(\vartheta) + q^4\check{B}_{2j}^{(1b)}(\vartheta)\right\} + \mathrm{O}(q^6)\,, \tag{56}$$

and

$$\sum_{\substack{j=-\infty \\ j\neq 0}}^{\infty} \check{b}_j\left\{\sigma\mathrm{e}^{\mathrm{i}j\vartheta} - \check{L}_j^{(2b)}(\vartheta)\right\} - \sum_{j=-\infty}^{\infty} \check{a}_j \check{L}_j^{(2a)}(\vartheta) = q^2\sum_{j=-\infty}^{\infty} \check{a}_j \check{B}_{1j}^{(2a)}(\vartheta), \tag{57}$$

where

$$\begin{cases} \check{L}_j^{(1a)}(\vartheta) = \check{L}_j^{(2b)}(\vartheta) = \mathrm{i}\frac{c}{J}\frac{j}{M}\mathrm{e}^{\mathrm{i}j\vartheta}, \quad \check{L}_j^{(1b)}(\vartheta) = \frac{1}{J}\frac{|j|}{M}\mathrm{e}^{\mathrm{i}j\vartheta}, \\ \check{L}_j^{(2a)}(\vartheta) = \left\{\alpha_0(\vartheta) - \mathrm{i}\frac{j}{M}\alpha_1(\vartheta) - \frac{j^2}{M^2}\alpha_2(\vartheta)\right\}\mathrm{e}^{\mathrm{i}j\vartheta}, \\ \check{B}_{1j}^{(1b)}(\vartheta) = \frac{M}{J}F_{1j}(\vartheta), \quad \check{B}_{2j}^{(1b)}(\vartheta) = \frac{M^3}{J}F_{2j}(\vartheta), \\ \check{B}_{1j}^{(2a)}(\vartheta) = -\sqrt{J}\,\mathrm{e}^{\mathrm{i}j\vartheta}. \end{cases} \tag{58}$$

Furthermore, we can expand the 2π-periodic functions $\check{L}_j^{(\cdot)}(\vartheta)$ and $\check{B}_{*j}^{(\cdot)}(\vartheta)$ in (56) and (57) in the form of Fourier series

$$\check{L}_j^{(\cdot)}(\vartheta) = \sum_{k=-\infty}^{\infty} \check{L}_{kj}^{(\cdot)}\,\mathrm{e}^{\mathrm{i}k\vartheta} \quad \text{and} \quad \check{B}_{*j}^{(\cdot)}(\vartheta) = \sum_{k=-\infty}^{\infty} \check{B}_{*kj}^{(\cdot)}\,\mathrm{e}^{\mathrm{i}k\vartheta}. \tag{59}$$

Substituting these into (56) and (57), we obtain

$$\sum_{k=-\infty}^{\infty}\left\{\sum_{j=-\infty}^{\infty}\check{a}_j\left(\sigma\delta_{kj} - \check{L}_{kj}^{(1a)}\right) - \sum_{\substack{j=-\infty\\ j\neq 0}}^{\infty}\check{b}_j\check{L}_{kj}^{(1b)}\right\}\mathrm{e}^{\mathrm{i}k\vartheta} = \sum_{k=-\infty}^{\infty}\left\{\sum_{\substack{j=-\infty\\ j\neq 0}}^{\infty}\check{b}_j\left(q^2\check{B}_{1kj}^{(1b)} + q^4\check{B}_{2kj}^{(1b)}\right)\right\}\mathrm{e}^{\mathrm{i}k\vartheta} + \mathrm{O}(q^6), \tag{60}$$

and

$$\sum_{k=-\infty}^{\infty}\left\{\sum_{\substack{j=-\infty\\ j\neq 0}}^{\infty}\check{b}_j\left(\sigma\delta_{kj} - \check{L}_{kj}^{(2b)}\right) - \sum_{j=-\infty}^{\infty}\check{a}_j\check{L}_{kj}^{(2a)}\right\}\mathrm{e}^{\mathrm{i}k\vartheta} = \sum_{k=-\infty}^{\infty}\left\{\sum_{j=-\infty}^{\infty}\check{a}_j q^2\check{B}_{1kj}^{(2a)}\right\}\mathrm{e}^{\mathrm{i}k\vartheta}, \tag{61}$$

where $\delta_{kj} = 0$ for $k \neq j$ and 1 for $k = j$. If a natural number M and a small value of q are given, this system of (60) and (61) approximately determines the linear stability due to disturbances for M different values of $p = K/M$ ($K = 0, 1, \dots, M-1$). As pointed out in Section 3.2.1, we can separate this combined system of (60) and (61) into M mutually exclusive systems corresponding to each value of $p = K/M$ ($K = 0, 1, \dots, M-1$) by changing j and k to $j_p(n) = -(Mn+K)$ and $j_p(m) = -(Mm+K)$, respectively, where $j_p(\cdot)$ is defined by (36). Then, the infinite series $\sum_{j=-\infty}^{\infty}$ and $\sum_{k=-\infty}^{\infty}$ in (60) and (61) are also replaced by $\sum_{n=-\infty}^{\infty}$ and $\sum_{m=-\infty}^{\infty}$, respectively, which can be truncated as

$$\sum_{n=-\infty}^{\infty} \sim \sum_{n=-N/2+1}^{N/2} \quad \text{and} \quad \sum_{m=-\infty}^{\infty} \sim \sum_{m=-N/2+1}^{N/2}, \tag{62}$$

where N is a large enough even number. From these, we can rewrite the separated system of (60) and (61) for $p = K/M$ in the matrix form

$$\sigma \boldsymbol{v} - L\boldsymbol{v} = q^2 B_1 \boldsymbol{v} \ + \ q^4 B_2 \boldsymbol{v} \ + \ \mathrm{O}(q^6) \qquad \text{for } \ p = K/M, \tag{63}$$

where

$$\boldsymbol{v} = \begin{pmatrix} \boldsymbol{a} \\ \boldsymbol{b} \end{pmatrix}, \tag{64}$$

and

$$L = \begin{pmatrix} L^{(1a)} & L^{(1b)} \\ L^{(2a)} & L^{(2b)} \end{pmatrix}, \quad B_1 = \begin{pmatrix} 0 & B_1^{(1b)} \\ B_1^{(2a)} & 0 \end{pmatrix}, \quad B_2 = \begin{pmatrix} 0 & B_2^{(1b)} \\ 0 & 0 \end{pmatrix}. \tag{65}$$

Here $\boldsymbol{a} = (a_{-N/2+1}, \dots, a_{N/2})^\top$, $\boldsymbol{b} = (b_{-N/2+1}, \dots, b_{N/2})^\top$, $L^{(\cdot)} = (L^{(\cdot)}_{mn})$, and $B^{(\cdot)}_{*} = (B^{(\cdot)}_{*mn})$, where $^\top$ denotes the transpose, $-N/2 + 1 \leq m, n \leq N/2$, and

$$\left. \begin{aligned} & a_n = \check{a}_{j=j_p(n)}, \quad b_n = \check{b}_{j=j_p(n)} \\ & L^{(\cdot)}_{mn} = \check{L}^{(\cdot)}_{k=k_p(m),\ j=j_p(n)}, \quad B^{(\cdot)}_{*mn} = \check{B}^{(\cdot)}_{*k=k_p(m),\ j=j_p(n)} \end{aligned} \right\}. \tag{66}$$

For $p = 0$ ($K = 0$), $\{j_p(n)\}_{n=-\infty}^{\infty} = \{-Mn\}_{n=-\infty}^{\infty}$ includes 0, but b_0 is omitted in $\boldsymbol{v}$ because $b_0 = 0$ from the bottom condition as shown in (35). Thus, for $p = 0$, $\boldsymbol{v}$ is a $2N - 1$ dimensional vector and L, B_1 and B_2 are $(2N-1) \times (2N-1)$ matrices. On the other hand, for $p \neq 0$, $\{j_p(n)\}_{n=-\infty}^{\infty}$ does not include 0, and thus $\boldsymbol{v}$ is a $2N$ dimensional vector and L, B_1 and B_2 are $2N \times 2N$ matrices. Also note that L, B_1 and B_2 depend on h and p.

4 | LINEAR STABILITY ANALYSIS USING A PERTURBATION THEORY FOR MATRICES

To apply a perturbation theory for matrices [Ref. 15, section 1.6] [16,17] to the linearized system (63) for small values of q, we introduce the perturbation parameter $\epsilon = q^2$ and rewrite (63) as

$$\sigma \boldsymbol{v} - L\boldsymbol{v} = \epsilon B_1 \boldsymbol{v} \ + \ \epsilon^2 B_2 \boldsymbol{v} \ + \ \mathrm{O}(\epsilon^3) \qquad \text{for } \ p = K/M \quad \text{ with } \ \epsilon = q^2. \tag{67}$$

We can approximately evaluate σ and $\boldsymbol{v}$ in (67) by expanding them in powers of ϵ^ν as

$$\left. \begin{aligned} \sigma &= \sigma^{(0)} + \varepsilon^{\nu}\sigma^{(1)} + \varepsilon^{2\nu}\sigma^{(2)} + \varepsilon^{3\nu}\sigma^{(3)} + \cdots \\ v &= v^{(0)} + \varepsilon^{\nu}v^{(1)} + \varepsilon^{2\nu}v^{(2)} + \varepsilon^{3\nu}v^{(3)} + \cdots \end{aligned} \right\}, \tag{68}$$

where ν (> 0) depends on the multiplicity of the eigenvalue $\sigma^{(0)}$ as a solution of the characteristic equation of the matrix L, as will be shown in Section 4.2.

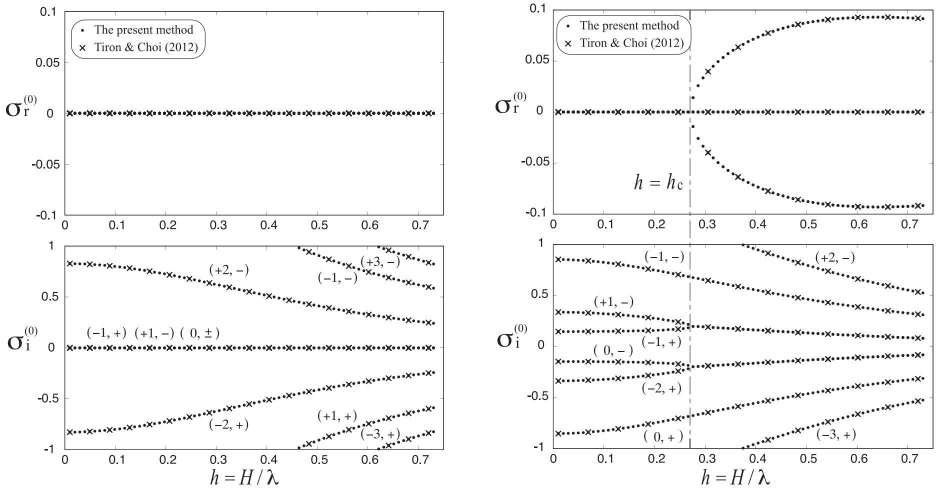

(a) $p = 0$ (b) $p = 1/2$

FIGURE 2 Variation of the eigenvalue $\sigma^{(0)} = \sigma_r^{(0)} + i\sigma_i^{(0)}$ for $q = 0$ in (69) with the wave steepness $h = H/\lambda$: (A) the superharmonic case $p = 0$ ($M = 1$, $K = 0$) and (B) the subharmonic case $p = 1/2$ ($M = 2$, $K = 1$). Each normal mode is labeled by $(n, \pm) = \sigma_n^{\pm}(p)$ defined by (70). In (B), the critical wave steepness $h_c \simeq 0.272108$. The computed results with $N = 128$ are compared with those of the two-dimensional stability analysis by Tiron and Choi[12]

4.1 | Two-dimensional linear stability for $q = 0$

In the absence of disturbances in the transverse direction, namely, for $q = 0$ ($\epsilon = 0$), the linearized system (67) becomes an eigenvalue problem given by

$$L\boldsymbol{v}^{(0)} = \sigma^{(0)}\boldsymbol{v}^{(0)} \qquad \text{for } p = K/M. \tag{69}$$

The eigenvalue $\sigma^{(0)}$ of the matrix L determines the two-dimensional linear stability due to disturbances in the propagation direction of steady waves with $p = K/M$. We numerically compute $\sigma^{(0)}$ and $\boldsymbol{v}^{(0)}$ in (69) using the computational routine "zgeev" in LAPACK (http://www.netlib.org/lapack/). Figures 2(A) and (B) show some computed results for the variation of the eigenvalue $\sigma^{(0)} = \sigma_r^{(0)} + i\sigma_i^{(0)}$ with the wave steepness $h = H/\lambda$ for (a) the superharmonic case $p = 0$ ($M = 1, K = 0$) and (b) the subharmonic case $p = 1/2$ ($M = 2, K = 1$), respectively. The number N of the truncated series in (62) is set to $N = 128$. Each eigenvalue is labeled by $(n, \pm)$ of the corresponding eigenvalue $\sigma_n^{\pm}(p) := \sigma_n^{\pm}(p, q = 0)$ in (25) in the zero-amplitude limit $h \to 0$ for $q = 0$, namely,

$$\sigma_n^{\pm}(p) = -i\{p + n \pm |p + n|^{3/2}\}. \tag{70}$$

The results in Figure 2 agree well with those by Tiron and Choi.[12]

In the superharmonic case of $p = 0$, as shown in Figure 2(A), the growth rate σ_r of the disturbance vanishes for the whole range of the wave steepness $0 \le h \le 0.73$, and thus the steady waves are always stable. On the other hand, in the subharmonic case of $p = 1/2$, as shown in Figure 2(B), the two pairs of eigenvalues, $(\sigma_{+1}^{-}, \sigma_{-1}^{+})$ and $(\sigma_0^{-}, \sigma_{-2}^{+})$, collide at $h = h_c \simeq 0.272108$, and the steady waves are unstable for $h > h_c$. In the following sections, we study the three-dimensional linear stability by adding the transverse disturbances to these two cases: $p = 0$ and $1/2$.

4.2 | Three-dimensional linear stability for small values of q

To obtain high-order eigensolutions $\sigma^{(\mu)}$ and $\boldsymbol{v}^{(\mu)}$ ($\mu = 1, 2, \ldots$) in (68), we introduce the left-eigenvector $\boldsymbol{u}^{(0)}$ and the Schur decomposition of the matrix L. The right- and left-eigenvectors, $\boldsymbol{v}_i^{(0)}$ and $\boldsymbol{u}_i^{(0)}$, corresponding to the i-th eigenvalue $\sigma_i^{(0)}$ of the matrix L satisfy

$$\begin{cases} L\boldsymbol{v}_i^{(0)} = \sigma_i^{(0)}\boldsymbol{v}_i^{(0)} \ , \\ \overline{\boldsymbol{u}}_i^{(0)\top} L = \sigma_i^{(0)}\overline{\boldsymbol{u}}_i^{(0)\top} \quad \text{or} \quad \overline{L}^{\top}\boldsymbol{u}_i^{(0)} = \overline{\sigma}_i^{(0)}\boldsymbol{u}_i^{(0)}. \end{cases} \tag{71}$$

Here, note that $\boldsymbol{v}_i^{(0)}$ and $\boldsymbol{u}_j^{(0)}$ have an orthogonality such that

$$\sigma_i^{(0)} \neq \sigma_j^{(0)} \quad \Rightarrow \quad \left(\boldsymbol{v}_i^{(0)}, \boldsymbol{u}_j^{(0)}\right) = 0. \tag{72}$$

The Schur decomposition [Ref. 20, p. 335] of the $2N \times 2N$ matrix L can be expressed as

$$L\boldsymbol{q}_j = \sigma_j^{(0)}\boldsymbol{q}_j + \sum_{i=1}^{j-1}\beta_{ij}\boldsymbol{q}_i \quad (j = 1, 2, \ldots, 2N), \tag{73}$$

where the Schur vectors $\boldsymbol{q}_j$ satisfy $(\boldsymbol{q}_i, \boldsymbol{q}_j) = 0$ for $i \neq j$.

4.2.1 | The superharmonic case ($p = 0$)

In the case of $p = 0$ ($M = 1$ and $K = 0$), L is a $(2N-1)\times(2N-1)$ matrix, as described at the end of Section 3.2.2. The eigenvalues $\sigma_i^{(0)}$ ($i = 1, 2, \ldots, 2N-1$) of L include a zero eigenvalue $\sigma_1^{(0)} = 0$ for all wave amplitudes, as shown in Figure 2(A), which is a triple root of the characteristic equation of the matrix L. Then, we consider the following case of the eigenvalues $\sigma_i^{(0)}$ ($i = 1, 2, \ldots, 2N-1$):

$$\begin{cases} \sigma_1^{(0)} = \sigma_2^{(0)} = \sigma_3^{(0)} = 0 \quad \text{and} \quad \sigma_i^{(0)} \neq 0 \ (i \geq 4), \\ \sigma_i^{(0)} \neq \sigma_j^{(0)} \ \ (i \neq j\ , \ \ i, j \geq 4). \end{cases} \tag{74}$$

Here, because $\sigma_n^{\pm}(p = 0) = -\mathrm{i}(n \pm |n|^{3/2})$ in (70), $\sigma_1^{(0)}$ and $\sigma_2^{(0)}$ correspond to the modes $\sigma_{n=1}^{-} = 0$ and $\sigma_{n=-1}^{+} = 0$, respectively, and $\sigma_3^{(0)}$ to the mode $\sigma_{n=0}^{\pm} = 0$. This condition (74) is satisfied for almost all wave amplitudes except at some finite number of values of h where there exist i and j ($i \neq j, i, j \geq 4$) such that $\sigma_i^{(0)} = \sigma_j^{(0)}$, as shown by Tiron and Choi [Ref. 12, figure 3 on p. 412].

The number of linearly independent eigenvectors corresponding to these three zero eigenvalues $\sigma_i^{(0)}$ ($i = 1, 2, 3$) in (74) are only two. Then, the Jordan decomposition of the matrix L can be

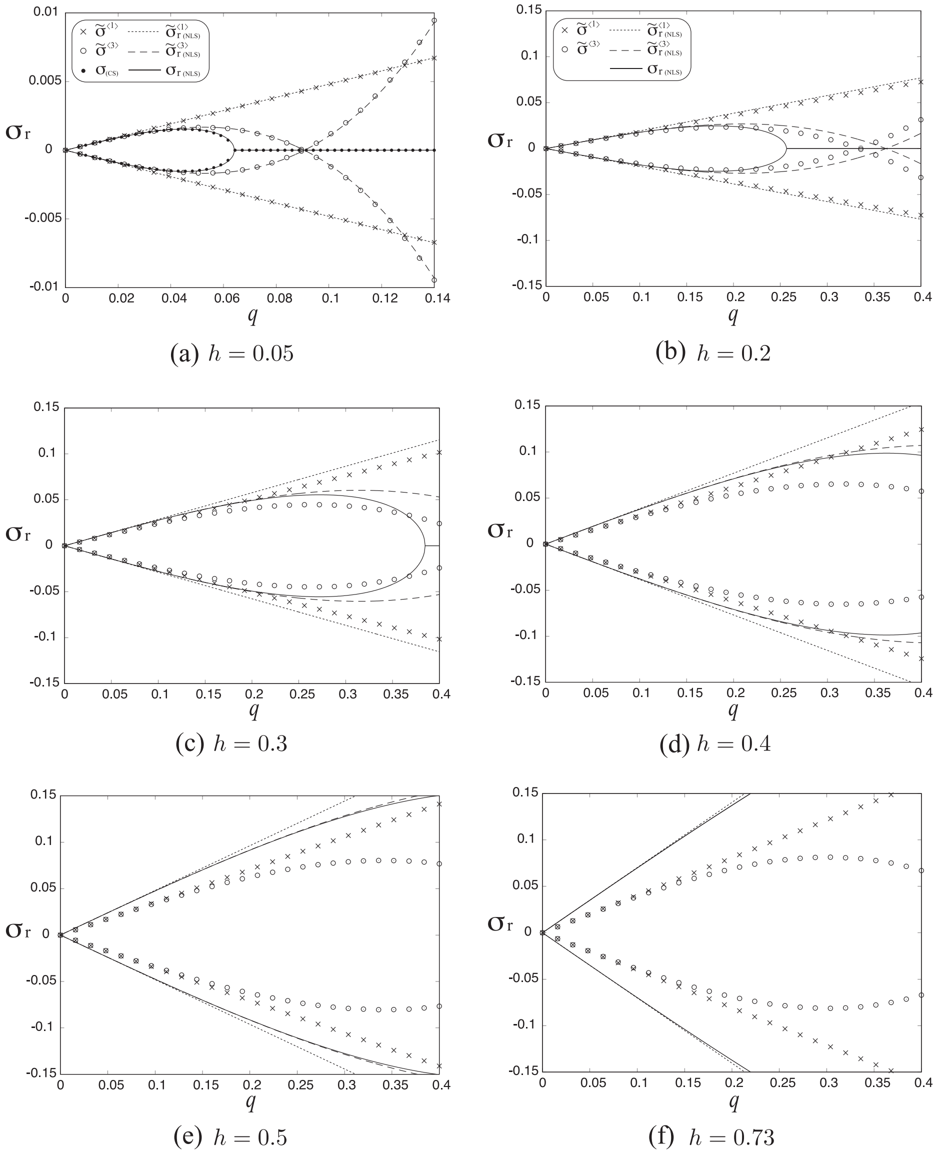

FIGURE 3 Variation of the growth rate σ_r with the transverse wavenumber q for the superharmonic case $p = 0$ ($M = 1, K = 0$). $\sigma = \sigma_r + i\sigma_i$: the eigenvalue and $h = H/\lambda$: the wave steepness. The first- and third-order approximations denoted by $\tilde{\sigma}^{\langle 1 \rangle}$ ($\times$) and $\tilde{\sigma}^{\langle 3 \rangle}$ ($\circ$) are computed using the present method (91), while $\tilde{\sigma}_{(CS)}$ ($\bullet$) in (A) is computed by using the method of Chen and Saffman.[4] The solution of the weakly nonlinear model $\sigma_{r(NLS)}$ (solid) is given by (92) while its first- and third-order approximations denoted by $\tilde{\sigma}^{\langle 1 \rangle}_{r(NLS)}$ (dotted) and $\tilde{\sigma}^{\langle 3 \rangle}_{r(NLS)}$ (dashed) are given by (94). The ranges of q and σ_r are $0 \le q \le 0.14$ and $|\sigma_r| < 0.01$ in (A), and $0 \le q \le 0.4$ and $|\sigma_r| < 0.15$ in (B)–(F). ($N = 128$)

expressed as [Ref. 15, section 1.6]

$$L\boldsymbol{v}_1^{(0)} = \sigma_1^{(0)}\boldsymbol{v}_1^{(0)} \quad \text{and} \quad L\boldsymbol{q}_2^{(0)} = \sigma_2^{(0)}\boldsymbol{q}_2^{(0)} + \beta_{12}\boldsymbol{v}_1^{(0)}, \tag{75}$$

and

$$L\boldsymbol{v}_i^{(0)} = \sigma_i^{(0)}\boldsymbol{v}_i^{(0)} \qquad (i = 3, 4, \dots, 2N-1), \tag{76}$$

where $\beta_{12} \in \mathbb{C}$ and $\boldsymbol{q}_2^{(0)}$ is the generalized eigenvector satisfying $(\sigma_2^{(0)}I - L)^2\boldsymbol{q}_2^{(0)} = \mathbf{0}$. Note that $\{\boldsymbol{v}_1^{(0)}, \boldsymbol{q}_2^{(0)}, \boldsymbol{v}_3^{(0)}, \boldsymbol{v}_4^{(0)}, \dots, \boldsymbol{v}_{2N-1}^{(0)}\}$ are linearly independent. From the perturbation theory for matrices [Ref. 15, section 1.6], the eigensolutions σ and $\boldsymbol{v}$ in (67) can be expanded in powers of $\epsilon^{1/2}$, namely, (68) with $\nu = 1/2$, around $\sigma^{(0)} = \sigma_1^{(0)} = 0$ and $\boldsymbol{v}^{(0)} = \boldsymbol{v}_1^{(0)}$. By substituting these expansions, Equation (67) can be approximated successively as

$$\left.\begin{array}{ll}
\mathrm{O}(\varepsilon^0) & : A_1\boldsymbol{v}_1^{(0)} = \mathbf{0} \\
\mathrm{O}(\varepsilon^{1/2}) & : A_1\boldsymbol{v}^{(1)} = -\sigma^{(1)}\boldsymbol{v}_1^{(0)} \\
\mathrm{O}(\varepsilon^1) & : A_1\boldsymbol{v}^{(2)} = -\sigma^{(1)}\boldsymbol{v}^{(1)} - \sigma^{(2)}\boldsymbol{v}_1^{(0)} + B_1\boldsymbol{v}_1^{(0)} \\
\mathrm{O}(\varepsilon^{3/2}) & : A_1\boldsymbol{v}^{(3)} = -\sigma^{(1)}\boldsymbol{v}^{(2)} - \sigma^{(2)}\boldsymbol{v}^{(1)} - \sigma^{(3)}\boldsymbol{v}_1^{(0)} + B_1\boldsymbol{v}^{(1)} \\
\mathrm{O}(\varepsilon^2) & : A_1\boldsymbol{v}^{(4)} = -\sigma^{(1)}\boldsymbol{v}^{(3)} - \sigma^{(2)}\boldsymbol{v}^{(2)} - \sigma^{(3)}\boldsymbol{v}^{(1)} - \sigma^{(4)}\boldsymbol{v}_1^{(0)} + B_1\boldsymbol{v}^{(2)} + B_2\boldsymbol{v}_1^{(0)}
\end{array}\right\}, \tag{77}$$

where

$$A_1 = \sigma_1^{(0)}I - L. \tag{78}$$

Here the 0-th order equation $A_1\boldsymbol{v}_1^{(0)} = \mathbf{0}$ corresponds to the two-dimensional linear stability problem (69). Taking the inner product of the both sides of (77) with the left-eigenvector $\boldsymbol{u}_1^{(0)}$ in (71), we obtain

$$\left(\boldsymbol{v}_1^{(0)}, \boldsymbol{u}_1^{(0)}\right) = 0 , \tag{79}$$

from the equation of $\mathrm{O}(\epsilon^{1/2})$. Then, using (79), the high-order equations determine $\sigma^{(1)}$, $\sigma^{(2)}$, and $\sigma^{(3)}$ in the form

$$\left.\begin{aligned}
\sigma^{(1)} &= \frac{(B_1\boldsymbol{v}_1^{(0)}, \boldsymbol{u}_1^{(0)})}{(\boldsymbol{v}^{(1)}, \boldsymbol{u}_1^{(0)})} \\
\sigma^{(2)} &= \frac{(B_1\boldsymbol{v}^{(1)}, \boldsymbol{u}_1^{(0)}) - \sigma^{(1)}(\boldsymbol{v}^{(2)}, \boldsymbol{u}_1^{(0)})}{(\boldsymbol{v}^{(1)}, \boldsymbol{u}_1^{(0)})} \\
\sigma^{(3)} &= \frac{(B_1\boldsymbol{v}^{(2)}, \boldsymbol{u}_1^{(0)}) + (B_2\boldsymbol{v}_1^{(0)}, \boldsymbol{u}_1^{(0)}) - \sigma^{(1)}(\boldsymbol{v}^{(3)}, \boldsymbol{u}_1^{(0)}) - \sigma^{(2)}(\boldsymbol{v}^{(2)}, \boldsymbol{u}_1^{(0)})}{(\boldsymbol{v}^{(1)}, \boldsymbol{u}_1^{(0)})}
\end{aligned}\right\}. \tag{80}$$

We can numerically obtain $\sigma^{(1)}$, $\sigma^{(2)}$ and $\sigma^{(3)}$ using the computational method in Appendix A.1.

4.2.2 | The subharmonic case ($p = 1/2$)

In the case of $p = 1/2$ ($M = 2$ and $K = 1$), L is a $2N \times 2N$ matrix, as described at the end of Section 3.2.2. We focus on the two eigenvalues $\sigma_1^{(0)}$ and $\sigma_2^{(0)}$ of L corresponding to the two modes $\sigma_{n=-1}^{+} \simeq 0 + 0.146446\,\mathrm{i}$ and $\sigma_{n=1}^{-} \simeq 0 + 0.337117\,\mathrm{i}$, respectively, where $\sigma_n^{\pm}$ is defined by (70). These two eigenvalues $\sigma_1^{(0)}$ and $\sigma_2^{(0)}$ collide at the critical wave steepness $h = h_c$ ($\simeq 0.272108$) as shown in Figure 2(B), namely, $\sigma_1^{(0)} = \sigma_2^{(0)}$, which is a multiple root of the characteristic equation of L at $h = h_c$. In particular, we examine the linear stability for h close to h_c. Therefore, the exponent ν of ϵ^{ν} in the perturbative expansion (68) depends on the wave steepness h.

For $h \neq h_c$, we consider the case of the eigenvalues $\sigma_i^{(0)}$ ($i = 1, 2, \dots, 2N$) of L being mutually different ($\sigma_i^{(0)} \neq \sigma_j^{(0)}$ for $i \neq j$). This condition is satisfied for h not so close to h_c. Then, the eigensolutions $\sigma = \sigma_i$ and $\boldsymbol{v} = \boldsymbol{v}_i$ ($i = 1, 2$) in (67) can be expanded in the form of (68) with $\nu = 1$ around $\sigma_i^{(0)}$ and $\boldsymbol{v}_i^{(0)}$ ($i = 1, 2$), respectively [Ref. 15, section 1.6]. Substituting these into (67), we can obtain at $\mathrm{O}(\epsilon^n)$ the equations for $\boldsymbol{v}_i^{(n)}$ for $n = 1, 2, 3$ as

$$\left.\begin{aligned} \mathrm{O}(\varepsilon^0) &: A_i \boldsymbol{v}_i^{(0)} = \boldsymbol{0} \\ \mathrm{O}(\varepsilon^1) &: A_i \boldsymbol{v}_i^{(1)} = -\sigma_i^{(1)} \boldsymbol{v}_i^{(0)} + B_1 \boldsymbol{v}_i^{(0)} \\ \mathrm{O}(\varepsilon^2) &: A_i \boldsymbol{v}_i^{(2)} = -\sigma_i^{(1)} \boldsymbol{v}_i^{(1)} - \sigma_i^{(2)} \boldsymbol{v}_i^{(0)} + B_1 \boldsymbol{v}_i^{(1)} + B_2 \boldsymbol{v}_i^{(0)} \end{aligned}\right\} \quad \text{for } h \neq h_c \quad (i = 1, 2), \tag{81}$$

where

$$A_i = \sigma_i^{(0)} I - L \quad (i = 1, 2). \tag{82}$$

Taking the inner product of the both sides of (81) with the left-eigenvector $\boldsymbol{u}_i^{(0)}$ in (71), we can write $\sigma_i^{(1)}$ and $\sigma_i^{(2)}$ in the form

$$\left.\begin{aligned} \sigma_i^{(1)} &= \frac{(B_1 \boldsymbol{v}_i^{(0)}, \boldsymbol{u}_i^{(0)})}{(\boldsymbol{v}_i^{(0)}, \boldsymbol{u}_i^{(0)})} \\ \sigma_i^{(2)} &= \frac{(B_1 \boldsymbol{v}_i^{(1)}, \boldsymbol{u}_i^{(0)}) + (B_2 \boldsymbol{v}_i^{(0)}, \boldsymbol{u}_i^{(0)}) - \sigma_i^{(1)} (\boldsymbol{v}_i^{(1)}, \boldsymbol{u}_i^{(0)})}{(\boldsymbol{v}_i^{(0)}, \boldsymbol{u}_i^{(0)})} \end{aligned}\right\} \quad \text{for } h \neq h_c \quad (i = 1, 2). \tag{83}$$

We can numerically obtain $\sigma_i^{(1)}$ and $\sigma_i^{(2)}$ using the computational method in Appendix A.2.

For $h \simeq h_c$, the accuracy of $\sigma_i^{(1)}$ and $\sigma_i^{(2)}$ ($i = 1, 2$) in (83) deteriorates, because $\sigma_1^{(0)} = \sigma_2^{(0)}$ at $h = h_c$ and thus, similarly to (79), the denominators $(\boldsymbol{v}_i^{(0)}, \boldsymbol{u}_i^{(0)})$ for $i = 1, 2$ in (83) approach zero as $h \to h_c$. Then we propose an alternative method using a local analysis near the critical point $h = h_c$ as follows. First, the Schur decomposition of the matrix L in (73) for $j = 1, 2$ can be written in the same form as (75), because $\boldsymbol{q}_1$ in (73) is equal to $\boldsymbol{v}_1^{(0)}$. Because $\sigma_1^{(0)} \simeq \sigma_2^{(0)}$ for $h \simeq h_c$, we may put

$$\sigma_2^{(0)} - \sigma_1^{(0)} = \epsilon^{1/2} \Delta\sigma \qquad \text{for } h \simeq h_c, \tag{84}$$

and rewrite (75) as

$$L\boldsymbol{v}_1^{(0)} = \sigma_1^{(0)}\boldsymbol{v}_1^{(0)} \quad \text{and} \quad L\boldsymbol{q}_2^{(0)} = \sigma_1^{(0)}\boldsymbol{q}_2^{(0)} + \beta_{12}\,\boldsymbol{v}_1^{(0)} + \epsilon^{1/2}\Delta\sigma\,\boldsymbol{q}_2^{(0)} \quad \text{for } h \simeq h_c. \tag{85}$$

The number of linearly independent eigenvectors corresponding to the eigenvlaue $\sigma_1^{(0)} = \sigma_2^{(0)}$ is only one at $h = h_c$. Then, we may assume that the eigensolutions σ and $\boldsymbol{v}$ for $h \simeq h_c$ can be expanded in the form of (68) with $\nu = 1/2$, and, similarly to (A2) in Appendix A.1, the equation of $O(\epsilon^{1/2})$ produces

$$\boldsymbol{v}^{(1)} = d_1^{(1)}\boldsymbol{v}_1^{(0)} + d_2^{(1)}\boldsymbol{q}_2^{(0)} \quad \text{and} \quad \sigma^{(1)} = d_2^{(1)}\beta_{12}. \tag{86}$$

Substituting these into the equation of $O(\epsilon^1)$, we get

$$A_1\boldsymbol{v}^{(2)} = -\left(\sigma^{(1)}d_1^{(1)} + \sigma^{(2)}\right)\boldsymbol{v}_1^{(0)} - d_2^{(1)}(\sigma^{(1)} - \Delta\sigma)\boldsymbol{q}_2^{(0)} + B_1\boldsymbol{v}_1^{(0)}. \tag{87}$$

Taking the inner product of both sides of (87) with the left-eigenvector $\boldsymbol{u}_1^{(0)}$ in (71), and using (86) and the orthogonality (79), we obtain a quadratic equation for $\sigma^{(1)}$, and its solution is given by

$$\sigma^{(1)} = \sigma_\pm^{(1)} := \frac{\Delta\sigma}{2} \pm \sqrt{\left(\frac{\Delta\sigma}{2}\right)^2 + \beta_{12}\frac{(B_1\boldsymbol{v}_1^{(0)}, \boldsymbol{u}_1^{(0)})}{(\boldsymbol{q}_2^{(0)}, \boldsymbol{u}_1^{(0)})}} \quad \text{for } h \simeq h_c. \tag{88}$$

Thus, the eigenvalue σ for $h \simeq h_c$ can be locally approximated by $\tilde{\sigma}_c = \sigma_1^{(0)} + \epsilon^{1/2}\sigma_\pm^{(1)}$ with $\epsilon = q^2$, namely,

$$\sigma \sim \tilde{\sigma}_c := \frac{\sigma_2^{(0)} + \sigma_1^{(0)}}{2} \pm \sqrt{\left(\frac{\sigma_2^{(0)} - \sigma_1^{(0)}}{2}\right)^2 + q^2\beta_{12}\frac{(B_1\boldsymbol{v}_1^{(0)}, \boldsymbol{u}_1^{(0)})}{(\boldsymbol{q}_2^{(0)}, \boldsymbol{u}_1^{(0)})}} \quad \text{for } h \simeq h_c. \tag{89}$$

5 | NUMERICAL RESULTS

This section shows some computed results of the approximate eigenvalue σ for small values of q obtained in §4 for both superharmonic ($p = 0$) and subharmonic ($p = 1/2$) disturbances. In these computations, the number N of the truncated series (62) is set to $N = 64$ or 128, and the computational routines “zgeev” and “zgees” in LAPACK (http://www.netlib.org/lapack/) are used for the left-eigenvector (71), the Schur decomposition in (73), and β_{12} in (75).

For relatively small-amplitude capillary waves, the weakly nonlinear models based on the formulation of the cubic nonlinear Schrödinger equation were derived in the previous studies [Ref. 4, eq. (2.20) on p. 131] [Ref. 6, eq. (2.10) on p. 309]. These models yield the approximate growth rate $\sigma_{r(NLS)}$ of the three-dimensional disturbances as

$$\sigma_{r(NLS)} = \mathrm{Re}\left\{\frac{3}{8}\sqrt{p^2 + 2q^2}\left(\frac{\pi^2}{3}h^2 - (p^2 + 2q^2)\right)^{1/2}\right\}, \tag{90}$$

where Re{·} denotes the real part. Here, note that this approximation is supposed to be valid for small h, p, and q. We compare this weakly nonlinear solution (90) with the present method.

5.1 | The superharmonic case ($p = 0$)

For the superharmonic case $p = 0$ ($M = 1$ and $K = 0$), we compute $\sigma^{(1)}$, $\sigma^{(2)}$, and $\sigma^{(3)}$ using the perturbative method in Section 4.2.1, and obtained the first- and third-order approximations $\tilde{\sigma}^{\langle 1\rangle}$ and $\tilde{\sigma}^{\langle 3\rangle}$ given by

$$\tilde{\sigma}^{\langle 1\rangle} := \sigma_1^{(0)} + \epsilon^{1/2}\sigma^{(1)} \quad \text{and} \quad \tilde{\sigma}^{\langle 3\rangle} := \sigma_1^{(0)} + \epsilon^{1/2}\sigma^{(1)} + \epsilon\sigma^{(2)} + \epsilon^{3/2}\sigma^{(3)}. \tag{91}$$

Here, note that $\sigma_1^{(0)} = 0$ and that the computed results of $\sigma^{(2)}$ almost vanish, namely, $\sigma^{(2)} \simeq 0$. Figure 3 shows some compute results of the variation of the growth rate σ_{r}, namely, the real part of $\tilde{\sigma}^{\langle 1\rangle}$ and $\tilde{\sigma}^{\langle 3\rangle}$, with q. These results demonstrate that, for the superharmonic disturbances ($p = 0$), Crapper's capillary waves are two-dimensionally stable for $q = 0$, but three-dimensionally unstable for long-wavelength disturbances in the transverse direction with $0 < q \ll 1$ for almost all wave amplitudes.

The present method cannot be applied to some finite number of values of the wave steepness h, for which multiple roots $\sigma_i^{(0)}$ ($i \geq 4$) other than the triple root $\sigma_1^{(0)}$ exists, as pointed out at the beginning of Section 4.2.1. However, the computed results of the growth rate σ_{r} change continuously with h. Thus, we may conjecture that the characteristics of the computed results in Figure 3 can be found for all wave amplitudes.

Figure 3 also compares the present results with those of Chen and Saffman.[4] It should be remarked that they formulated the three-dimensional linear stability problem in the physical space and expanded the solutions in the rectangular coordinate system (x_1, x_2, y) in Figure 1(A) using Floquet theory. Their method does not require any assumptions for p and q, but its application is limited to small-amplitude waves due to the slow convergence of the expansion as the amplitude increases. Computed results for the eigenvalue $\tilde{\sigma}_{(\mathrm{CS})}$ using their method are shown for $h = 0.05$ by the black circle points in Figure 3(A), but no convergent solutions can be obtained for $h \geq 0.1$. Therefore, no computed eigenvalues using the method of Chen and Saffman[4] are presented for $h \geq 0.1$ in the following.

In addition, for the superharmonic case ($p = 0$), the weakly nonlinear solution $\sigma_{\mathrm{r(NLS)}}$ in (90) becomes

$$\sigma_{\mathrm{r(NLS)}} = \mathrm{Re}\left\{\frac{3}{4}q\left(\frac{\pi^2}{6}h^2 - q^2\right)^{1/2}\right\}. \tag{92}$$

This agrees well for small-amplitude waves with the computed results for $\tilde{\sigma}_{(\mathrm{CS})}$ of Chen and Saffman,[4] as shown in Figure 3(A). For $q \ll h$, $\sigma_{\mathrm{r(NLS)}}$ in (92) can be expanded as

$$\sigma_{\mathrm{r(NLS)}} = \frac{\sqrt{6}\pi}{8}hq\left\{1 - \frac{1}{2}\frac{6}{\pi^2}\left(\frac{q}{h}\right)^2 - \frac{1}{8}\left(\frac{6}{\pi^2}\right)^2\left(\frac{q}{h}\right)^4 - \cdots\right\} \qquad \text{for } \frac{q}{h} \ll 1, \tag{93}$$

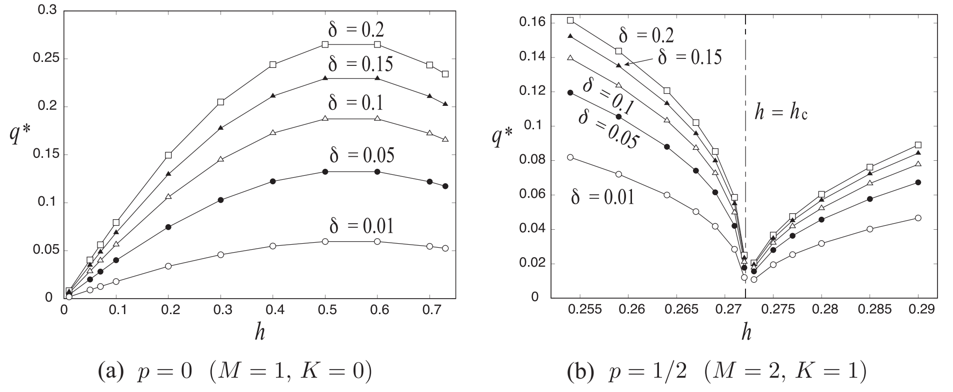

FIGURE 4 Variation of the upper limit q^* of the valid range $0 \le q \le q^*$ with the wave steepness $h = H/\lambda$. The valid range with q^* and δ is defined by (95) for the superharmonic case ($p = 0$) and (97) for the subharmonic case ($p = 1/2$). In (B), $h = h_c \simeq 0.272108$: the critical wave steepness (see Figure 2(B)). ($N = 128$)

and the leading- and next-order approximations to (93) are given, using $\epsilon = q^2$, by

$$\tilde{\sigma}^{\langle 1\rangle}_{\mathrm{r(NLS)}} = \epsilon^{1/2}\sigma^{(1)}_{\mathrm{r(NLS)}} \quad \text{and} \quad \tilde{\sigma}^{\langle 3\rangle}_{\mathrm{r(NLS)}} = \epsilon^{1/2}\sigma^{(1)}_{\mathrm{r(NLS)}} + \epsilon^{3/2}\sigma^{(3)}_{\mathrm{r(NLS)}}, \tag{94}$$

where $\sigma^{(1)}_{\mathrm{r(NLS)}} = (\sqrt{6}\pi/8)h$ and $\sigma^{(3)}_{\mathrm{r(NLS)}} = -\{3\sqrt{6}/(8\pi)\}(1/h)$. Figure 3 demonstrates that the computed results $\tilde{\sigma}^{\langle 1\rangle}$ and $\tilde{\sigma}^{\langle 3\rangle}$ in (91) using the present method agree well for small values of h and q with $\tilde{\sigma}^{\langle 1\rangle}_{\mathrm{r(NLS)}}$ and $\tilde{\sigma}^{\langle 3\rangle}_{\mathrm{r(NLS)}}$ in (94), respectively, but the difference between them increases with h. In particular, the weakly nonlinear NLS model overestimates the growth rate as h increases.

In the present method, the wavenumber q in the transverse direction is assumed to be small. To estimate the range of validity of q as $0 \le q \le q^*$, we introduce the convergence rate of the expansion of σ in (68) that is defined, for a small value of δ, by

$$\frac{|\tilde{\sigma}^{\langle 1\rangle} - \tilde{\sigma}^{\langle 3\rangle}|}{|\tilde{\sigma}^{\langle 1\rangle}|} < \delta \qquad \text{for } 0 \le q \le q^*. \tag{95}$$

Figure 4(A) shows the upper limit q^* for different small values of δ in (95). It is found that the range of validity narrows with decrease of h, or $q^* \to 0$ as $h \to 0$. This result confirms that the present method is valid for $q/h \ll 1$, as observed in the comparison of our numerical results with the NLS solution (93). Nevertheless, the present method can describe the stability characteristics over the whole amplitude range as long as q is less than q^*, which increases with h.

5.2 | The subharmonic case ($p = 1/2$)

For the subharmonic case $p = 1/2$ ($M = 2$ and $K = 1$), we compute $\sigma^{(1)}_i$ and $\sigma^{(2)}_i$ ($i = 1, 2$) using the perturbation method described in Section 4.2.2. First, for $h \ne h_c$, we define the first- and second-order approximations $\tilde{\sigma}^{\langle 1\rangle}_i$ and $\tilde{\sigma}^{\langle 2\rangle}_i$ ($i = 1, 2$) as

$$\tilde{\sigma}^{\langle 1\rangle}_i := \sigma^{(0)}_i + \epsilon\sigma^{(1)}_i \quad \text{and} \quad \tilde{\sigma}^{\langle 2\rangle}_i := \sigma^{(0)}_i + \epsilon\sigma^{(1)}_i + \epsilon^2\sigma^{(2)}_i \quad (i = 1, 2) \quad \text{for } h \ne h_c, \tag{96}$$

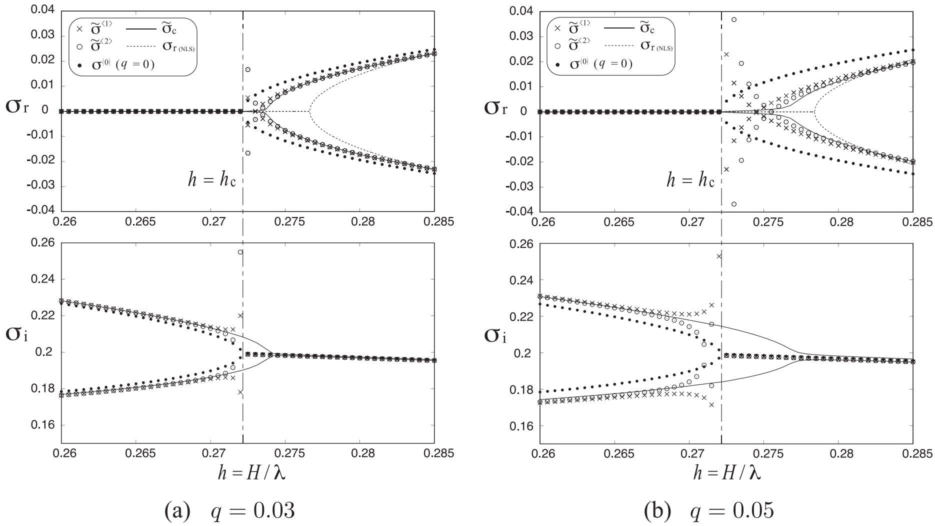

FIGURE 5 Variation of the eigenvalue $\sigma = \sigma_r + i\sigma_i$ with the wave steepness $h = H/\lambda$ near the critical point $h = h_c$ for the subharmonic case $p = 1/2$ ($M = 2$, $K = 1$). (A) $q = 0.03$ and (B) $q = 0.05$. $\times$: $\tilde{\sigma}_m^{\langle 1\rangle}$ and $\circ$: $\tilde{\sigma}_m^{\langle 2\rangle}$ ($m = 1, 2$) in (96) for $h \neq h_c$. $\bullet$: $\sigma^{(0)}$ ($q = 0$). The critical wave steepness h_c is computed to be $h_c \simeq 0.272108$ (see Figure 2(B)). Notice that the computed results with $N = 64$ become inaccurate near the critical wave amplitude h_c, but the local solution $\tilde{\sigma}_c$ (solid line) given by (89) provides more accurate results for $h \simeq h_c$. The weakly nonlinear solution $\sigma_{r(NLS)}$ (dotted line) given by (90) inaccurately predicts the shift of the critical wave steepness h_c

where $\sigma_1^{(0)}$ and $\sigma_2^{(0)}$ correspond to the two modes $\sigma^+_{n=-1}$ and $\sigma^-_{n=1}$, respectively, as defined at the beginning of Section 4.2.2. We compute $\sigma_i^{(1)}$ and $\sigma_i^{(2)}$ ($i = 1, 2$) in (96) using (83) and (A17), respectively. Figures 5(A) and (B) compare the variation of the eigenvalue $\sigma = \sigma_r + i\sigma_i$ with the wave steepness h for $q = 0.03$ and 0.05, respectively. These computations are performed with $N = 64$, where N is the number of the truncated series (62). The results in Figure 5 demonstrate that the long-wavelength disturbances in the transverse direction slightly reduce the growth rate σ_r of the two-dimensionally unstable waves for $h > h_c$ ($\simeq 0.272108$), but accuracy of $\tilde{\sigma}_i^{\langle 1\rangle}$ and $\tilde{\sigma}_i^{\langle 2\rangle}$ ($i = 1, 2$) in (96) deteriorates for h close to h_c, as pointed out in Section 4.2.2. It is, however, found that this inaccuracy for $h \simeq h_c$ is improved by the local solution $\tilde{\sigma}_c$ in (89), which is shown by the solid line in Figure 5. Note that the weakly nonlinear solution $\sigma_{r(NLS)}$ in (90) denoted by the dotted line in Figure 5 inaccurately describes the shift of the critical amplitude for $q \neq 0$.

To examine the relation between the growth rate σ_r and the transverse wavenumber q in more detail, we compare some computed results for the variation of σ_r with q for a range of values of h near the criticality, as shown in Figure 6. In these computations, N is set to 128. It is found that (i) for $h > h_c$, the growth rate σ_r of the two-dimensionally unstable waves decreases with q, and (ii) for $h < h_c$, Crapper's capillary waves are still stable ($\sigma_r = 0$) even under weakly three-dimensional disturbances. Also, we can see that the local solution $\tilde{\sigma}_c$ for $h \simeq h_c$ in (89) agrees with $\tilde{\sigma}_i^{\langle 2\rangle}$ ($i = 1, 2$) in (96) well for small values of q.

Similarly to (95) for the superharmonic case, we define the range of validity as $0 \leq q \leq q^*$ for the subharmonic case with

$$\frac{|\tilde{\sigma}_s^{\langle 1\rangle} - \tilde{\sigma}_s^{\langle 2\rangle}|}{|\tilde{\sigma}_s^{\langle 1\rangle}|} < \delta \qquad \text{for } 0 \leq q \leq q^*, \tag{97}$$

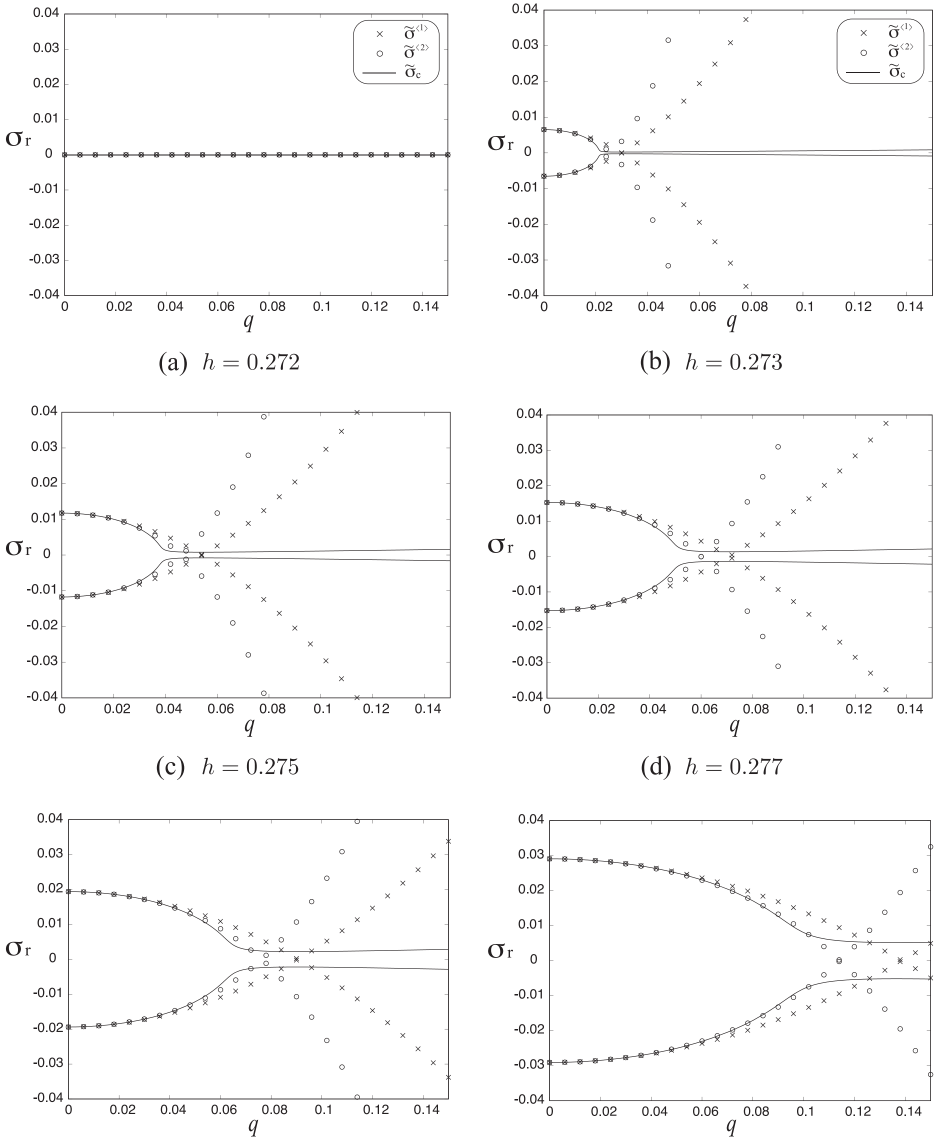

(a) $h = 0.272$

(b) $h = 0.273$

(c) $h = 0.275$

(d) $h = 0.277$

(e) $h = 0.28$

(f) $h = 0.29$

FIGURE 6 Variation of the growth rate σ_r with the transverse wavenumber q near the critical amplitude for the subharmonic case $p = 1/2$ ($M = 2, K = 1$). $\sigma = \sigma_\mathrm{r} + \mathrm{i}\sigma_\mathrm{i}$: the eigenvalue and $h = H/\lambda$: the wave steepness. $\times$: the first-order approximation $\tilde{\sigma}_m^{\langle 1\rangle}$ and $\circ$: the second-order approximation $\tilde{\sigma}_m^{\langle 2\rangle}$ ($m = 1, 2$) in (96) for $h \neq h_\mathrm{c}$. The solid line : the local solution $\tilde{\sigma}_\mathrm{c}$ in (89) for $h \simeq h_\mathrm{c}$. $h = h_\mathrm{c} \simeq 0.272108$: the critical wave steepness (see Figure 2(B)). ($N = 128$)

where $\tilde{\sigma}_s^{\langle\mu\rangle} = \mathrm{Im}\{\tilde{\sigma}_1^{\langle\mu\rangle}\}$ for $h < h_\mathrm{c}$ and $\tilde{\sigma}_s^{\langle\mu\rangle} = \mathrm{Re}\{\tilde{\sigma}_1^{\langle\mu\rangle}\}$ for $h > h_\mathrm{c}$ ($\mu = 1, 2$). Figure 4(B) shows that, for $p = 1/2$, the upper limit q^* in (97) approaches zero as $h \to h_\mathrm{c}$. This result is consistent with the deterioration of accuracy of $\sigma_i^{(1)}$ and $\sigma_i^{(2)}$ ($i = 1, 2$) in (83) for $h \simeq h_\mathrm{c}$, which is pointed out in Section 4.2.2.

6 | CONCLUSIONS

We have considered the three-dimensional linear stability of the periodic motion of pure capillary waves progressing in permanent form with constant speed on water of infinite depth. We have introduced the coordinate transformation (11) using Crapper's solution (8) to study the stability for the whole range of wave amplitudes. To solve the linearized equations (15), (16), (17), and (18) for small disturbances added to the steady capillary waves in the transformed space, we have assumed that the wavenumber p of the disturbances in the propagation direction of Crapper's capillary waves is a rational number given by (27), and that the wavenumber q of the disturbances in the direction transverse to the propagation direction is small, namely, the wavelength in the transverse direction being long. These assumptions and the periodicity of each variable allow us to transform the linearized equations for disturbances into the matrix form (63) of an eigenvalue problem.

We have focused on the superharmonic case of $p = 0$ and the subharmonic case of $p = 1/2$, and have developed a computational method to obtain approximate eigensolutions to the linearized system (63), following a perturbation theory for matrices, as shown in Section 4. In this perturbative method, the eigenvalue σ and the eigenvector $\boldsymbol{v}$ in (63) are expanded in powers of ϵ^{ν} $(= q^{2\nu})$ around the unperturbed solutions $\sigma^{(0)}$ and $\boldsymbol{v}^{(0)}$ for $q = 0$ in the form of (68), where the exponent ν depends on the multiplicity of $\sigma^{(0)}$ as a solution of the characteristic equation of the matrix L of the eigenvalue problem (69). Using the orthogonality of the left- and right eigenvectors and the Schur decomposition of the matrix L, we can numerically obtain the high-order eigensolutions $\sigma^{(\mu)}$ and $\boldsymbol{v}^{(\mu)}$ $(\mu = 1, 2, \ldots)$ in (68). Using this method, we have successfully computed the growth rate $\sigma_{\rm r}$, or the real part of the eigenvalue $\sigma = \sigma_{\rm r} + {\rm i}\sigma_{\rm i}$ for the whole range of wave amplitudes. In previous studies, it was computed only for relatively small-amplitude waves.

For the superharmonic case with $p = 0$, the numerical examples have demonstrated that the steady capillary waves are two-dimensionally stable for $q = 0$, but are three-dimensionally unstable for the long-wavelength disturbances with $0 < q \ll 1$ for almost all wave amplitudes. For small-amplitude waves $(0 < h \ll 1)$, our results agree with the approximate solution (92) of the weakly nonlinear model, but have shown the reduced growth rate for finite amplitude waves.

The subharmonic case with $p = 1/2$ requires two different approaches for $h \neq h_{\rm c}$ and $h \simeq h_{\rm c}$, with $h = h_{\rm c}$ being the critical wave steepness for $q = 0$, where the corresponding eigenvalue is a double root of the characteristic equation of the matrix L. The computed results using the approach for $h \neq h_{\rm c}$ showed that the long-wavelength disturbances in the transverse direction reduce the growth rate $\sigma_{\rm r}$ of two-dimensionally unstable waves for $h > h_{\rm c}$. The accuracy of our solutions using this approach deteriorates as $h \to h_{\rm c}$, but, for $h \simeq h_{\rm c}$, can be improved by the local analysis discussed in Section 4.2.2.

ACKNOWLEDGMENTS

We thank Dr. Y. Watanabe of Kyushu University and Dr. K. Tanaka of the University of Tokyo for helpful discussions on numerical computation. The work of S.M. was supported by JSPS KAKENHI grant no. JP17H02856 and the Research Institute for Mathematical Sciences, an International Joint Usage/Research Centre located in Kyoto University. W.C. gratefully acknowledges support from the U.S. National Science Foundation through grant no. OCE-1634939.

ORCID

Sunao Murashige https://orcid.org/0000-0002-8393-9739
Wooyoung Choi https://orcid.org/0000-0002-4433-3013

REFERENCES

1. McLean JW. Instabilities of finite-amplitude water waves. *J. Fluid Mech*. 1982;114:315-330.
2. Kharif C, Ramamonjiarisoa A. On the stability of gravity waves on deep water. *J. Fluid Mech*. 1990;218:163-170.
3. Francius M, Kharif C. Three-dimensional instabilities of periodic gravity waves in shallow water. *J. Fluid Mech*. 2006;561:417-437.
4. Chen B, Saffman PG. Three-dimensional stability and bifurcation of capillary and gravity waves on deep water. *Stud. Appl. Math*. 1985;72:125-147.
5. Zhang J, Melville WK. Three-dimensional instabilities of nonlinear gravity-capillary waves. *J. Fluid Mech*. 1987;174:187-208.
6. Dias F, Kharif C. Nonlinear gravity and capillary-gravity waves. *Annu. Rev. Fluid Mech*. 1999;31:301-346.
7. Crapper GD. An exact solution for progressive capillary waves of arbitrary amplitudes. *J. Fluid Mech*. 1957;2:532-540.
8. Longuet-Higgins MS. The instabilities of gravity waves of finite amplitude in deep water. I. Superharmonics. *Proc. R. Soc. Lond. A*. 1978;360:471-488.
9. Longuet-Higgins MS. The instabilities of gravity waves of finite amplitude in deep water. II. Subharmonics. *Proc. R. Soc. Lond. A*. 1978;360:489-505.
10. Tanaka M. The stability of steep gravity waves. *J. Phys. Soc. Japan*. 1983;52:3047-3055.
11. Hogan SJ. The superharmonic normal mode instabilities of nonlinear deep-water capillary waves. *J. Fluid Mech*. 1988;190:165-177.
12. Tiron R, Choi W. Linear stability of finite-amplitude capillary waves on water of infinite depth. *J. Fluid Mech*. 2012;696:402-422.
13. Murashige S, Choi W. Stability analysis of deep-water waves on a linear shear current using unsteady conformal mapping. *J. Fluid Mech*. 2020;885:A41.
14. Kataoka T, Tsutahara M. Transverse instability of surface solitary waves. *J. Fluid Mech*. 2004;512:211-221.
15. Hinch EJ. *Perturbation Methods*. Cambridge, MA: Cambridge University Press; 1991.
16. Kato T. *Perturbation Theory for Linear Operators*. Berlin-Heidelberg-New York: Springer-Verlag, Reprint of the 1980 edition; 1995.
17. Baumgärtel H. *Analytic Perturbation Theory for Matrices and Operators*. Basel-Boston-Stuttgart: Birkhäuser-Verlag; 1985.
18. Hildebrand FB. *Advanced Calculus for Applications*. 2nd ed., Englewood Cliffs, NJ: Prentice Hall; 1976.
19. King FW. *Hilbert Transforms*. *Encyclopedia of Mathematics and Its Applications 124*., Vol. 1. Cambridge, MA: Cambridge University Press; 2009.
20. Golub GH, Van Loan CF. *Matrix Computations*. Baltimore, MD: Johns Hopkins University Press; 1989.

How to cite this article: Murashige S, Choi W. Linear stability of transversely modulated finite-amplitude capillary waves on deep water. *Stud Appl Math*. 2021;146:498–525. https://doi.org/10.1111/sapm.12353

APPENDIX A: COMPUTATIONAL METHODS OF THE HIGH-ORDER EIGENVALUES IN (80) AND (83)

A.1 | The superharmonic case ($p = 0$)

For the numerical evaluation of $\sigma^{(\mu)}$ ($\mu = 1, 2, 3$), each equation in (80) can be further transformed as follows. First, $\boldsymbol{v}^{(\mu)}$ ($\mu = 1, 2, 3$) can be represented by the linear combination of

$\{\boldsymbol{v}_1^{(0)}, \boldsymbol{q}_2^{(0)}, \boldsymbol{v}_3^{(0)}, \boldsymbol{v}_4^{(0)}, \dots, \boldsymbol{v}_{2N-1}^{(0)}\}$ as

$$\boldsymbol{v}^{(\mu)} = d_1^{(\mu)}\boldsymbol{v}_1^{(0)} + d_2^{(\mu)}\boldsymbol{q}_2^{(0)} + \sum_{k=3}^{2N-1} d_k^{(\mu)}\boldsymbol{v}_k^{(0)} \qquad (\mu = 1, 2, 3)\ , \tag{A1}$$

Substituting (A1) for $\mu = 1$ into the equation of $O(\epsilon^{1/2})$ in (77) and using the second equation in (75) and $\sigma_1^{(0)} = \sigma_2^{(0)} = 0$, we obtain

$$\boldsymbol{v}^{(1)} = d_1^{(1)}\boldsymbol{v}_1^{(0)} + d_2^{(1)}\boldsymbol{q}_2^{(0)} + d_3^{(1)}\boldsymbol{v}_3^{(0)} \quad \text{and} \quad \sigma^{(1)} = d_2^{(1)}\beta_{12}. \tag{A2}$$

Using these results and the orthogonality (72) and (79), the first equation for $\sigma^{(1)}$ in (80) can be rewritten as

$$\{\sigma^{(1)}\}^2 = \beta_{12}\frac{(B_1\boldsymbol{v}_1^{(0)}, \boldsymbol{u}_1^{(0)})}{(\boldsymbol{q}_2^{(0)}, \boldsymbol{u}_1^{(0)})}. \tag{A3}$$

Next, using $\boldsymbol{v}^{(1)}$ in (A2), $B_1\boldsymbol{v}^{(1)}$ can be decomposed as

$$B_1\boldsymbol{v}^{(1)} = d_1^{(1)}B_1\boldsymbol{v}_1^{(0)} + d_2^{(1)}B_1\boldsymbol{q}_2^{(0)} + d_3^{(1)}B_1\boldsymbol{v}_3^{(0)}, \tag{A4}$$

and each term on the right-hand side can be represented, similarly to (A1), by

$$\begin{cases} B_1\boldsymbol{v}_i^{(0)} = e_{i1}\boldsymbol{v}_1^{(0)} + e_{i2}\boldsymbol{q}_2^{(0)} + \displaystyle\sum_{k=3}^{2N-1} e_{ik}\boldsymbol{v}_k^{(0)} \qquad (i = 1, 3), \\ B_1\boldsymbol{q}_2^{(0)} = e_{21}\boldsymbol{v}_1^{(0)} + e_{22}\boldsymbol{q}_2^{(0)} + \displaystyle\sum_{k=3}^{2N-1} e_{2k}\boldsymbol{v}_k^{(0)}. \end{cases} \tag{A5}$$

Here, we can obtain the coefficients e_{ik} ($i = 1, 2, 3$ and $k = 1, 2, \dots, 2N-1$) in (A5) using the orthogonality conditions (72) and (79) as

$$\begin{cases} e_{i2} = \dfrac{(B_1\boldsymbol{v}_i^{(0)}, \boldsymbol{u}_1^{(0)})}{(\boldsymbol{q}_2^{(0)}, \boldsymbol{u}_1^{(0)})} \quad (i = 1, 3)\ , \quad e_{22} = \dfrac{(B_1\boldsymbol{q}_2^{(0)}, \boldsymbol{u}_1^{(0)})}{(\boldsymbol{q}_2^{(0)}, \boldsymbol{u}_1^{(0)})}, \\ e_{ik} = \dfrac{(\boldsymbol{w}_i, \boldsymbol{u}_k^{(0)})}{(\boldsymbol{v}_k^{(0)}, \boldsymbol{u}_k^{(0)})} \quad (i = 1, 2, 3 \quad \text{and} \quad k = 3, 4, \dots, 2N-1), \\ e_{i1} = \dfrac{(\boldsymbol{w}_i, \boldsymbol{v}_1^{(0)}) - \sum_{k=3}^{2N-1} e_{ik}(\boldsymbol{v}_k^{(0)}, \boldsymbol{v}_1^{(0)})}{(\boldsymbol{v}_1^{(0)}, \boldsymbol{v}_1^{(0)})} \quad (i = 1, 2, 3), \end{cases} \tag{A6}$$

where

$$\boldsymbol{w}_i = B_1\boldsymbol{v}_i^{(0)} - e_{i2}\boldsymbol{q}_2^{(0)} \quad (i = 1, 3)\ , \quad \boldsymbol{w}_2 = B_1\boldsymbol{q}_2^{(0)} - e_{22}\boldsymbol{q}_2^{(0)}. \tag{A7}$$

Substituting $\boldsymbol{v}^{(2)}$ in (A1) and $B_1\boldsymbol{v}_1^{(0)}$ in (A5) into the equation of $O(\epsilon^1)$ in (77), we get

$$\begin{cases} d_2^{(1)}\sigma^{(1)} = e_{12}, \ \ d_3^{(1)}\sigma^{(1)} = e_{13}\,, \ \ d_2^{(2)}\beta_{12} = d_1^{(1)}\sigma^{(1)} + \sigma^{(2)} - e_{11}, \\ d_k^{(2)}\sigma_k^{(0)} = -e_{1k} \quad (k = 4, 5, \dots, 2N-1). \end{cases} \tag{A8}$$

The second equation in (A2) and the first equation in (A8) yield $\{\sigma^{(1)}\}^2 = \beta_{12}e_{12}$. From these, the second equation for $\sigma^{(2)}$ in (80) can be rewritten as

$$\sigma^{(2)} = \frac{1}{2}\left(e_{11} + e_{22} + \frac{e_{13}e_{32}}{e_{12}}\right). \tag{A9}$$

Furthermore, substituting $\boldsymbol{v}^{(3)}$ in (A1) and $B_1\boldsymbol{v}^{(1)}$ in (A4) into the equation of $O(\epsilon^{3/2})$ in (77), we get

$$\begin{cases} d_3^{(2)}\sigma^{(1)} = -d_3^{(1)}\sigma^{(2)} + d_1^{(1)}e_{13} + d_2^{(1)}e_{23} + d_3^{(1)}e_{33}, \\ d_2^{(3)}\beta_{12} = d_1^{(2)}\sigma^{(1)} + d_1^{(1)}\sigma^{(2)} + \sigma^{(3)} - d_1^{(1)}e_{11} - d_2^{(1)}e_{21} - d_3^{(1)}e_{31}. \end{cases} \tag{A10}$$

From these, the third equation for $\sigma^{(3)}$ in (80) can be rewritten as

$$\begin{aligned} \sigma^{(3)} = \frac{1}{2\sigma^{(1)}}\Bigg[& e_{12}e_{21} - (e_{11} - \sigma^{(2)})(e_{22} - \sigma^{(2)}) + e_{13}e_{31} - (e_{11} - \sigma^{(2)})(e_{33} - \sigma^{(2)}) \\ & + e_{23}e_{32} - (e_{22} - \sigma^{(2)})(e_{33} - \sigma^{(2)}) \\ & + \beta_{12}\left\{ \frac{(B_2\boldsymbol{v}_1^{(0)}, \boldsymbol{u}_1^{(0)})}{(\boldsymbol{q}_2^{(0)}, \boldsymbol{u}_1^{(0)})} - \sum_{k=4}^{2N-1} \frac{1}{\sigma_k^{(0)}} e_{1k}e_{k2} \right\}\Bigg], \end{aligned} \tag{A11}$$

where

$$e_{k2} = \frac{(B_1\boldsymbol{v}_k^{(0)}, \boldsymbol{u}_1^{(0)})}{(\boldsymbol{q}_2^{(0)}, \boldsymbol{u}_1^{(0)})} \qquad (k = 4, 5, \dots, 2N-1). \tag{A12}$$

We can compute $\sigma^{(1)}$, $\sigma^{(2)}$, and $\sigma^{(3)}$ using (A3), (A9), and (A11), respectively.

A.2 | The subharmonic case ($p = 1/2$)

For numerical evaluation, $\sigma_i^{(2)}$ in (83) can be further transformed as follows. First, $\boldsymbol{v}_i^{(1)}$ and $B_1\boldsymbol{v}_i^{(0)}$ ($i = 1, 2$) can be represented by the linear combination of $\{\boldsymbol{v}_1^{(0)}, \boldsymbol{v}_2^{(0)}, \boldsymbol{v}_3^{(0)}, \boldsymbol{v}_4^{(0)}, \dots, \boldsymbol{v}_{2N}^{(0)}\}$, respectively:

$$\boldsymbol{v}_i^{(1)} = \sum_{k=1}^{2N} d_{ik}\boldsymbol{v}_k^{(0)} \quad \text{and} \quad B_1\boldsymbol{v}_i^{(0)} = \sum_{k=1}^{2N} e_{ik}\boldsymbol{v}_k^{(0)} \qquad (i = 1, 2). \tag{A13}$$

We can obtain e_{mk} in (A13) using the orthogonality (72) as

$$e_{ik} = \frac{(B_1\boldsymbol{v}_i^{(0)}, \boldsymbol{u}_k^{(0)})}{(\boldsymbol{v}_k^{(0)}, \boldsymbol{u}_k^{(0)})} \qquad (i = 1, 2 \quad \text{and} \quad 1 \leq k \leq 2N). \tag{A14}$$

From the first equation in (83), we have

$$\sigma_i^{(1)} = e_{ii} \qquad (i = 1, 2). \tag{A15}$$

Substituting (A13) into the equation of $O(\epsilon^1)$ in (81) determines d_{ik} $(i \neq k)$ as

$$d_{ik} = \frac{e_{ik}}{\sigma_i^{(0)} - \sigma_k^{(0)}} \qquad (i \neq k). \tag{A16}$$

From these, we can rewrite the second equation in (83) as

$$\sigma_i^{(2)} = \frac{1}{(\boldsymbol{v}_i^{(0)}, \boldsymbol{u}_i^{(0)})}\left\{\sum_{\substack{k=1\\k\neq i}}^{2N} \frac{e_{ik}}{\sigma_i^{(0)} - \sigma_k^{(0)}} \cdot \left(B_1\boldsymbol{v}_k^{(0)}, \boldsymbol{u}_i^{(0)}\right) + \left(B_2\boldsymbol{v}_i^{(0)}, \boldsymbol{u}_i^{(0)}\right)\right\} \qquad (i = 1, 2). \tag{A17}$$

We can compute $\sigma_i^{(1)}$ and $\sigma_i^{(2)}$ $(i = 1, 2)$ using the first equation in (83) and (A17), respectively.